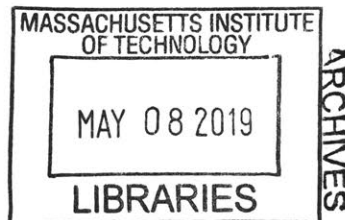Modeling life cycle greenhouse gas emissions from photovoltaic and wind power generation, with and without energy storage

by

Ian Miller
B.A., Government
Georgetown University, 2009

Submitted to the MIT Department of Chemical Engineering in Partial Fulfillment of the
Requirements for the Degree

of

Master of Science in Chemical Engineering

at the

Massachusetts Institute of Technology

~~February 2019~~ [June 2019]

Signature of Author _____ **Signature redacted**

MIT Department of Chemical Engineering
December 12th, 2018

Certified by _____ **Signature redacted**

Robert Armstrong
Director, MIT Energy Initiative
Chevron Professor of Chemical Engineering
Thesis Supervisor

Certified by _____ **Signature redacted**

William Green
Hoyt C. Hottel Professor of Chemical Engineering
Department Reader

Accepted by _____ **Signature redacted**

Patrick Doyle
Robert T. Haslam Professor of Chemical Engineering
Graduate Officer

Modeling life cycle greenhouse gas emissions from photovoltaic and wind power generation, with and without energy storage

by

Ian Miller

Submitted to the MIT Department of Chemical Engineering on December 12th, 2018 in Partial Fulfillment of the Requirements for the Degree of Master of Science in Chemical Engineering

ABSTRACT

From 2008 to 2016, photovoltaic (PV) power generation grew by a factor of 28 and changed significantly. Practices that were minor, including solar tracking, inverter overloading, and Chinese module manufacturing, became mainstream. Countries including the US and India installed large amounts of solar in warm regions with mean temperatures above 20 °C. The impacts of these developments on greenhouse gas (GHG) emissions from PV have not been analyzed by life cycle assessment (LCA) in depth. This thesis helps to fill that gap. The metric of life cycle GHG emissions per unit AC electricity supplied to grid is referred to here as "carbon intensity." The unit of grams-CO_2-equivalent/kilowatthour is abbreviated to g_C/kWh.

Several approximate findings are made on the carbon intensity of PV power. (1) Reversible temperature effects raise the carbon intensity of silicon PV power installed in warm regions, including by ~10% in the southwestern US and ~13% in western India. (2) All temperature effects raise silicon PV carbon intensity by ~23% in southern India (from 35 to 43 g_C/kWh). (3) Chinese manufacturing of multi-crystalline silicon (mc-Si) modules emits ~25% more GHGs than European manufacturing, due not only to higher carbon intensity of upstream electricity, as previously reported, but also to more energy input per module produced. (4) Relative to stationary mounting, tracking decreases the carbon intensity of mc-Si PV in most regions analyzed (by 0 to ~12%, or 0 to ~4 g_C/kWh), and increases the carbon intensity of cadmium telluride PV in most regions analyzed (by 0 to ~12%, or 0 to ~4 g_C/kWh). This dependence on cell type is explained by the interaction of tracking energy gain, tracker production emissions, and module production emissions. (5) Inverter overloading slightly diminishes PV carbon intensity, by less than 2 g_C/kWh.

This thesis also presents a simple model for estimating emissions from integrated power generation and energy storage. The model applies to emissions of all pollutants, not only GHGs, and to all storage technologies, including pumped hydroelectric. Our case study applies the model to systems that couple PV and wind generation with lithium-ion batteries (LBs) and vanadium redox flow batteries (VFBs). We find that, even when coupled with large amounts of LBs or VFBs, PV and wind power remain much less carbon intensive than fossil-based generation. The most carbon intensive renewable power analyzed (sc-Si PV produced in China, installed in Berlin, and coupled with sufficient VFBs to store 50% of generation) still emits only ~25% of the GHGs of the least carbon intensive mainstream fossil power (combined cycle gas turbine with no storage).

Lastly, we find that the pathway to minimize GHG emissions of power from a coupled system depends upon the generator: given low-emission generation (<50 g_C/kWh), the minimizing pathway is the storage technology with lowest production emissions (VFBs over LBs for our case study); given high-emission generation (>200 g_C/kWh), the minimizing pathway is the storage technology with highest round-trip efficiency (LBs over VFBs). The latter case applies to a majority of the world's power generation today.

Thesis Supervisor: Robert Armstrong
Title: Director, MIT Energy Initiative; Chevron Professor of Chemical Engineering

Contents

1. Introduction and literature review

1.1. Background

The electric power sector produced 40% of global greenhouse gas (GHG) emissions in 2015 [1]. To limit human-caused global warming to 2°C, the IEA projects that power sector emissions must decline to 11% of 2015 levels by 2050, from 13 to 1.4 gigatons of carbon dioxide per year [1]. To help achieve this decline, many governments have increased their support for low-carbon power sources. Due to this support and large cost reductions [2], photovoltaic (PV) and wind power have grown from ~1% of global electricity in 2007 to ~6% in 2017 [3], and are projected to reach 15-33% by 2040 [4,5]. The most widely deployed PV cell types are multi-crystalline silicon (mc-Si), single-crystalline silicon (sc-Si), and cadmium telluride (CdTe), with market shares of 70%, 24%, and 4%, respectively, of new PV installed in 2016 [6]. The most widely deployed wind turbines are 1.6-3 MW models installed at onshore wind farms, with generation from larger offshore turbines comprising a small but growing share of the total (5% in 2017) [7,8].

While the operating GHG emissions of PV and wind power are negligible, their upstream emissions are not. To be concise, this thesis refers to total life cycle GHG emissions of AC electricity as "carbon intensity", and the units of grams-CO_2-equivalent/kilowatthour as "g_C/kWh". The carbon intensity of PV power has been estimated at 76, 53, and 27 g_C/kWh for sc-Si, mc-Si, and CdTe PV, respectively, installed in northern Europe circa 2015, and at 33, 22, and 13 g_C/kWh for PV installed in the US southwest circa 2015 [9]. The carbon intensity of wind power has been estimated at approximately 12, 10, and 9 g_C/kWh, respectively, for onshore wind farms in low, medium, and high wind-speed areas, and at 14 g_C/kWh for offshore wind farms (which typically are located in high wind-speed areas) [10–18]. For context, representative GHG emissions from combined cycle natural gas (CCNG) and supercritical pulverized coal power (SCPC) are approximately 490 and 960 g_C/kWh, respectively [19].

The leading method for estimating carbon intensity is life cycle assessment (LCA). As outlined by ISO standards 14040 and 14044 [20], LCA quantifies a product's environmental impacts through input-output accounting of cradle-to-grave or cradle-to-gate processes. Since 2007, over 50 studies have conducted

LCA of PV power systems, and have found that the top drivers of PV carbon intensity are upstream electricity source, cell type, module efficiency, irradiance at installation site, and system lifetime [21,22]. Peng et al. [21] provided a detailed literature review of PV LCA and underlined gaps in the field, including the treatment of cell temperature and module orientation. IEA reports from 2008, 2011, and 2016 [23] provided methodology guidelines for PV LCA, and recommended that practitioners quantify emissions on a per AC kilowatthour basis, thus facilitating comparison to other power sources.

1.2. Motivation for PV LCA

While growing from less than 0.1% of global electricity in 2007 to over 1.5% in 2017 [3], PV power production has also changed significantly, as described below. Some of these changes have not been analyzed by LCA at all or in depth. This thesis aims to help fill that gap. In particular, we analyze the impact on PV carbon intensity of several practices that were minor in 2007 and are mainstream now, namely, inverter overloading, solar tracking, and Chinese mc-Si module production. In addition, we analyze the emissions impact of geographic temperature variation. Analyzing these impacts requires more detailed models of PV performance than PV LCAs have typically employed, including the use of temperature-dependent performance ratios. This thesis incorporates PV performance modelling via the use of capacity factors calculated with PVWatts, a software tool from the US National Renewable Energy Laboratory (NREL) [24].

The inverter loading ratio (ILR) of a PV system is the ratio of rated DC module capacity to rated AC inverter capacity. Inverter overloading is the practice of installing more module capacity than inverter capacity, thus yielding an ILR above 1. In the US, the mean ILR of new large-scale PV projects (AC capacity >1MW) rose from 1.09 in 2009 to 1.25 in 2016, while the share of new projects with ILRs of 1.4 or more grew from 0% to 23% (112 of 478 new projects in 2016) [8]. While inverter overloading has become the norm for PV power, its impact on PV carbon intensity has not been analyzed in the LCA literature.

As solar tracking becomes more common, estimating its emissions impacts becomes more relevant. Utility-scale PV (AC capacity >5MW) increasingly employs tracking, including 53% of cumulative and 70% of new capacity in the US in 2016 [8]. In the US from 2008 to 2014, under 20% of new utility-scale (AC capacity >5MW) CdTe projects had tracking (16 of 86 projects); in 2015 and 2016, the number was 56% (44 of 79 projects), including locations outside the exceptionally sunny US southwest, such as Colorado, Tennessee, and Georgia [8]. Several LCAs analyzed the emissions impact of solar tracking, but with limited geographic scope and tracking set-ups that are not (and do not claim to be) representative of industry practice [25–27]. Bayod-Rújula [25] analyzed a 2-axis tracking system in Spain. Beylot et al. [27] and Desideri et al. [26] analyzed hypothetical 1-axis tracking systems with 30° tilt in southern europe. In contrast, the industry norm for PV tracking is horizontal 1-axis tracking; in the US in 2016, 97% of utility-scale tracking PV projects used horizontal 1-axis tracking (255 of 263 projects) [28].

Two PV LCAs did analyze industry-representative tracking set-ups. Leccisi et al. [9] found that horizontal 1-axis tracking reduced carbon intensity by 11% and 1% for mc-Si and CdTe PV, respectively, installed in the US southwest. The study's abstract stated that "one-axis tracking installations can improve the environmental profile of PV systems by approximately 10% for most impact metrics," and did not mention location. Similarly, Sinha et al. [29] estimated that tracking reduced the carbon intensity of CdTe PV by 3% in the US southwest, and concluded that "tracking systems...provide an eco-efficient strategy for improving the sustainability of PV systems." However, neither study calculated tracking's impact outside the US southwest. Single-location results cannot support the generality of these statements, especially as tracking spreads in other less sunny regions. This thesis aims to build on these studies by calculating tracking's impact on PV carbon intensity over a range of locations.

The impact of temperature variation is relevant when calculating PV carbon intensity in any location, and especially relevant when comparing intensities across different climates. Several LCAs analyzed PV across regions with large mean temperature differences (>15 °C) [9,30,31]. A common approximation in these studies is temperature-independent performance ratio (PR). Perpiñan et al. [30] assumed constant cell temperature between central France and the central Sahara desert. Nian [31] assumed constant per-

formance ratio across northern Europe, the Middle East, Japan, Australia, the northern US, and Singapore. Leccisi et al. [9] assumed constant performance ratio between northern Europe and the US southwest. In contrast, actual PV performance ratios are understood to vary significantly and predictably with temperature. High temperatures reduce module operating efficiency and thus PR, both reversibly (via voltage decrease) [32] and irreversibly (via corrosion, discoloration, micro-cracking from thermal cycling, and other mechanisms) [33]. A typical silicon module's efficiency reversibly declines by ~0.47% (relative) for every 1°C increase in cell temperature. This relation between efficiency and temperature is based on statistical analysis of performance data from over 11,000 modules [24], and is widely assumed in modern PV performance modeling. Irreversible efficiency reduction (degradation) from high temperatures is less well characterized but can be a similar order of magnitude over a typical system lifetime [34]. Whether reversible or irreversible, efficiency drops decrease power output, and thereby increase the carbon intensity of PV power (g_C/kWh). This study estimates the extent of such increases.

1.3. Motivation for modeling emissions from coupled generation and storage

A barrier to continued growth of both PV and wind power, and one reason that projections span a large range, is intermittency, and uncertainties over how intermittency will be managed as renewables grow. Sunshine intensity and thus PV generation often do not align with electricity demand. For example, in California, solar generation starts declining in the mid-afternoon even as total demand (residential, commercial, and industrial) typically rises. As PV rises above 20% of average daily generation in a region, intermittency can lead to curtailment of existing PV, less favorable economics for future PV, and inefficient "peaker" use of other power systems, including gas-fired turbines [35,36]. "Peaker" power plants are only used to meet peak demand and otherwise are idle. Similar dynamics apply to wind at high penetration, albeit with more regional and temporal variation [37,38]. For example, in Texas, average wind power production peaks between 12 AM and 1 AM.

Energy storage can contribute to solving the challenges of intermittency. Storage coupled with generation has the potential to (1) flatten power supplied by intermittents to the grid, and (2) reduce the peak

power and thus capacity required of non-intermittents. Partly due to this potential, the growth of non-hydro storage capacity in the US has been accelerating, from ~1000 MWh added between 2013 and 2017, to a projected ~1000 MWh in 2018, and more in each year through 2023 [39]. Lithium-ion batteries (LBs) and vanadium redox flow batteries (VFBs) are two of the most common non-hydro storage types. LBs constitute a large majority of current and projected non-hydro storage deployment [39]. VFBs constitute a significant share of utility-scale storage installations with durations over 3 hours [40]. Storage duration is the ratio of rated storage energy capacity to rated storage power capacity, and represents the time required to discharge the fully charged storage unit at its rated power output. This thesis focuses on storage applications that require durations of 3 to 7 hours, such as smoothing intermittent generation to better match demand.

While coupling storage with generation can mitigate intermittency, the impact on the GHG emissions of electricity supply is less well understood. Spanos et al [41] conducted cradle-to-gate LCAs of lead-acid, nickel-zinc and manganese dioxide-zince batteries, and thus estimated their GHG emissions per battery mass produced. The authors did not analyze operating life or the coupling of batteries with generation. Rydh and Sandén [42] evaluated energy required to produce eight common battery types, including LBs, VRBs, lead-acid batteries (LABs), and sodium sulfur batteries (SSBs), and found that LBs require significantly more energy to produce than LABs or VRBs on a per energy capacity basis. Denholm et al [43] analyzed the coupling of generation with VRBs, pumped hydro storage (PHS), and compressed air energy storage (CAES). The authors found that electricity from nuclear or renewables coupled with PHS had lower carbon intensity than electricity from nuclear or renewables coupled with VRBs or CAES. On the other hand, with fossil generation, systems employing CAES had significantly lower GHG emissions than those with VRBs or PHS. Denholm et al and Mitavachan et al [44] both emphasized that the carbon intensity of electricity from a coupled system depended on both generation type and energy storage type.

This thesis complements these prior works by presenting a simple exploitable model to estimate emissions from a combined generation and storage system. The model applies to emissions of all pollutants,

not just GHGs, and to all storage, not just electrochemical. As a case study, we use the model to estimate the impact of adding LBs and VFBs to typical mainstream PV, wind, gas, and coal-based generation.

2. Methodology

2.1. PV LCA methodology

We developed a PV LCA modeling tool [45] following the ISO 14040 and 14044 standards [46] and the IEA PV LCA guidelines [23]. Table 1 summarizes how our analysis corresponds to these guidelines. In addition to elaborating several items in Table 1, this section describes how the modeling tool operates. We refer to the tool as SoLCAT (Solar Life Cycle Assessment Tool). To estimate GHG emissions from PV power, SoLCAT integrates four main elements: published PV life cycle inventories (LCIs), background emission factors from the Ecoinvent database [47], known physical correlations (e.g., the relation between rated module efficiency and capacity), and capacity factors from PVWatts, a software tool from the US National Renewable Energy Laboratory (NREL).

Table 1
Summary of correspondence of SoLCAT to IEA PV LCA methodology guidelines [23].

Item recommended by IEA guidelines	Value in this analysis
Goals of analysis	Estimating the GHG emissions intensity (carbon intensity) of PV power. Estimating how PV carbon intensity is impacted by inverter overloading, solar tracking, geographic temperature variation, and Chinese mc-Si module production.
LCA approach	Process-based LCA, also called attributional LCA.
LCA software tool	Tool built and presented here (SoLCAT). See methodology.
LCI databases used	Ecoinvent database V3. [47]
Impact indicator method used	IPCC 2013 GWP 100a.
Life cycle stages included	Raw material acquisition through power plant operation. See life cycle diagrams in Figure 1 and Figure 2. EOL of power plant is not included in emissions calculations due to lack of data.
PV cell type	Variable. Possible values include: sc-Si, mc-Si, CdTe, and CIGS.
Installation type	Variable. Possible values include: utility-scale fixed-tilt, utility-scale with horizontal 1-axis tracking, rooftop optimal tilt, rooftop "typical" tilt.
Rated efficiency	Variable.
Degradation rate (%/yr)	Variable.
Lifetime of modules	Variable. Consistent with LCI data sources [48,49], module losses are assumed at 1% during installation, and 2% over 30 years of operation (0.067% per year) due to module damages beyond linear degradation.
Lifetime of BOS	For inverters, 15 years. For mounting, module lifetime. Storage lifetime dependent on cycle life and use, as described in section 2.2.3.
Location of installation	Variable.
Annual irradiance (kWh / m² / yr)	Variable. In this analysis, incident irradiance depends on location, installation type (via orientation), and other model inputs. See capacity factor and appendix.
Module orientation	Variable and determined by installation type. Possible values include: -optimal orientation (equator facing, and irradiance-maximizing tilt, which can deviate from latitude tilt, e.g. by -9° in Berlin). This orientation is employed by the installation options "utility-scale fixed-tilt" and "rooftop optimal tilt"; -time-varying orientation, i.e. 1-axis east-west tracking with horizontal tilt & 45° rotation limit. -"typical" rooftop orientation (28° tilt and ± 45° deviation from equator facing);
Annual electricity production	Variable. Value depends on location, orientation, and other model inputs. See capacity factor section and appendix on performance modeling.
Performance ratio (PR)	Variable. PR is not assumed constant across locations or time, due to temperature differences, snow, and other effects. This is an important aspect of this work.
Region of production modeled	Variable. Possible values include: China (for mc-Si), Europe (for mc-Si and sc-Si), Malaysia (for CdTe), and Japan (for CIGS). Carbon intensity of upstream electricity, a model input, influences this item because certain carbon intensities are characteristic of certain regions.
Upstream electricity source	Variable, via variation of model inputs, namely, carbon intensities of upstream electricity used to make module & BOS.

---

[1] "Typical" is in quotes because this tilt and azimuth are based on those found common among PV-suitable rooftops in an NREL survey of ~23% of buildings in the continental US [67]. SW and SE azimuths occur at roughly equal levels in the buildings surveyed, and thus the capacity factor utilized by SoLCAT for a "typical" rooftop orientation in a location is the avg. of two capacity factors, one for 28° tilt and -45° deviation from equator-facing, and one for 28° tilt and +45° deviation from equator-facing. These capacity factor pairs differ minimally, by at most 2% at high latitude (e.g. London), 1% at medium latitude (e.g. Boston), and 0% at low latitude (e.g. Singapore).

2.1.1. PV LCA - Goal, system boundary, and functional unit

The primary goal of our PV LCA is estimating how the life cycle GHG emissions of PV power are impacted by inverter overloading, solar tracking, geographic temperature variation, and Chinese mc-Si module production. Our system is electricity production by PV. Electricity production can be considered a black box that consumes resources and produces electricity and emissions. The system's primary function is producing electricity, and thus the functional unit is a kilowatthour of AC electricity supplied to the grid. In addition to electricity, the other system output we analyze in the case study is GHG emissions. These two system outputs are combined into our central metric: GHGs emitted per AC electricity generated (g_C/kWh), referred to as "carbon intensity" in this thesis.

PV electricity production can be elaborated as shown in Figures 1 and 2. Commercial thin film module production is relatively less complex and more vertically integrated [48,50], and is not further segmented beyond Figure 1. Crystalline silicon module production is further elaborated in Figure 2.
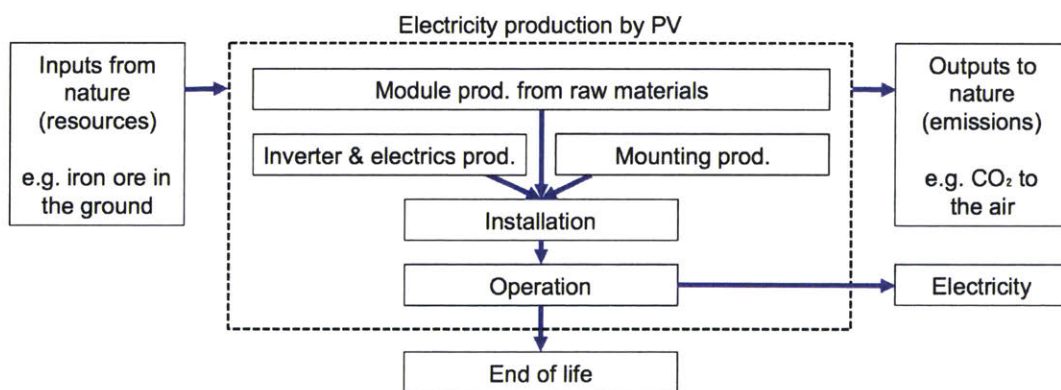

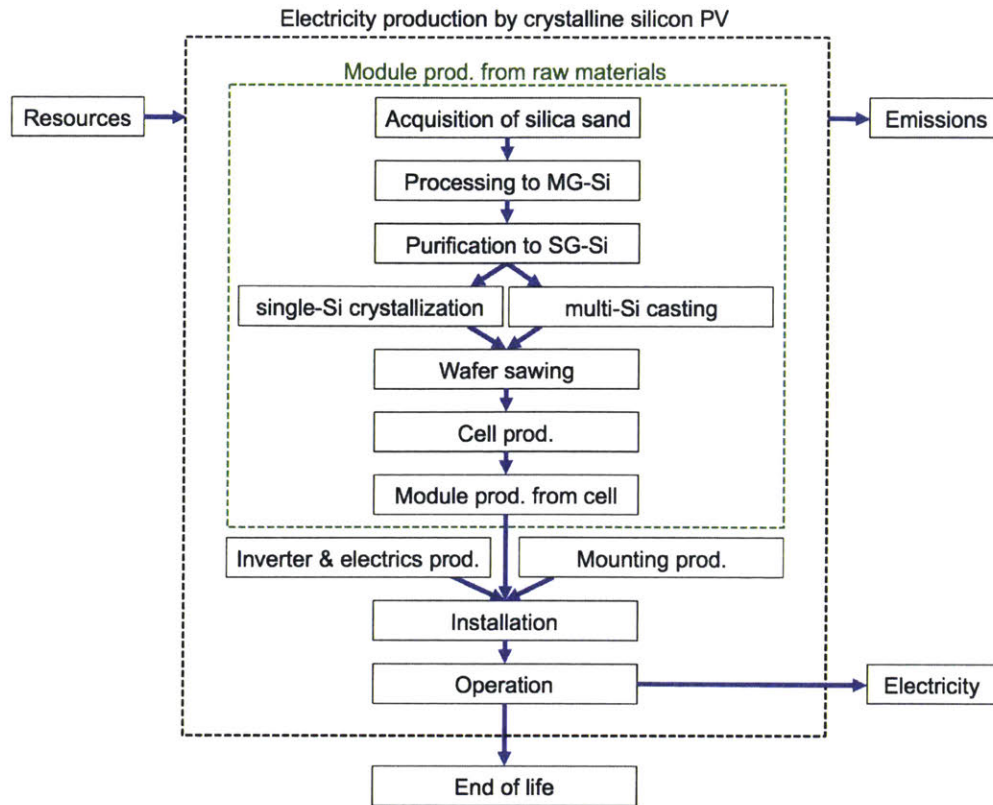Figure 1. Life cycle stages of PV electricity production.

Figure 2. Life cycle stages of electricity production by crystalline silicon PV.

LCA refers to the explicit stages in Figure 1 and Figure 2 as the "foreground" and their implied component processes as the "background". It should be emphasized that background processes, though not explicitly drawn, are inside the system border and include: production of chemicals used in silicon processing, construction and operation of module-manufacturing infrastructure, and raw material extraction processes (e.g., iron ore acquisition) that "pull" resources from nature, across the system boundary, and into the electricity production system. In this analysis, transport is treated as a background process that contributes to multiple foreground stages. For example, chemicals are transported to the site of silicon processing, and solar glass is transported to the site of module production. In other words, like materials and energy, transport is treated as an input to each stage. To be consistent, when the output of foreground process A is input to foreground process B, transport of the item is considered part of process B. Given multiple valid ways of segmenting life cycle and inputs, and the possibility that different segmentations

provide different insights, SoLCAT reports emissions breakdowns both by life cycle stage (cell production emissions, installation emissions, etc.) and by foreground input category (electricity emissions, transport emissions, etc.). Processes not included in our system include electricity transmission from generation site to end-use, and displacement of competing power sources.

2.1.2. PV LCA - Data sources

A list quantifying inputs and outputs of a stage is called a life cycle inventory (LCI). Our primary sources for PV foreground LCIs are the IEA's 2015 Report "Life Cycle Inventories & Life Cycle Assessments of PV Systems" [49] and the ESU's 2012 Report "Life Cycle Inventories of Photovoltaics" [48]. These sources aggregate large numbers of LCIs and explicitly aim to represent production typical of the PV industry. The IEA report provides "mainstream" and "best technology" LCIs for Chinese mc-Si module production. The mainstream LCIs are utilized in our model, while the best technology LCIs are used in a sensitivity analysis.. Other sources for foreground LCIs are the Ecoinvent Database V3 [47] for an LCI of silica sand acquisition, and Sinha et al. [29] for an LCI of a horizontal 1-axis tracking system.

To calculate life cycle GHG emissions from PV electricity, data is needed not just on foregrond LCIs but also on emission factors for hundreds of background processes. Our primary source for these data is the Ecoinvent V3 database [47]. The impact assessment method used by Ecoinvent V3 and thus by our model to calculate emission factors in units of CO_2-equivalent is IPCC 2013 GWP 100a [51].

The PV LCI sources used here are the most comprehensive available, but have two features which potentially constrain the applicability of our model. First, the IEA LCIs [49] utilize industry data collected before 2015. For the Chinese mc-Si LCIs, approximately half the data are from 2014 and half from 2011. The 2014 data include electricity inputs to all life stages, and a majority of inputs to casting, wafer production, and solar-grade Si production. The 2011 data are mainly material inputs to metallurgical-grade (MG) Si production and module assembly. It is unlikely that more recent surveys of MG-Si production would significantly affect our results because MG-Si production (1) is a carbothermic reduction process that is technologically mature and has been used by non-PV industries including electronics for over 50

years, and (2) emits little (<5%) of silicon PV's life cycle carbon, and a majority of this small share comes from using electricity, for which our model uses more recent data. In total, the 2014 Chinese mc-Si data accounts for ~75% of life cycle carbon emissions.[2] The IEA LCIs for European mc-Si, sc-Si, and thin film production use older data, published in 2014 by de Wild-Scholten [52], but collected from industry in 2011. The pre-2015 age of all foreground LCI data is mitigated by the use of more recent data on back-ground inputs (via Ecoinvent) and electricity sources (via annual IEA reports on electricity emissions by country [53]). Additionally, average wafer thickness and silicon usage per module capacity have been approximately constant since 2008 and 2012 [6], respectively, suggesting that 2011 and 2014 foreground data on wafer and module production remain applicable.

Second, the referenced LCIs do not provide data on end of life (EOL), partly because the large majority of PV installed has not reached its end of life. In the absence of data, our model does not account for emissions from PV EOL processes. Wind power LCAs face a similar lack of EOL data, but benefit from more established recycling processes for wind's primary materials (steel from towers, fiber glass from blades, etc.).

2.1.3. PV LCA - Model structure

SoLCAT uses foreground LCIs and background emissions factors in several ways to estimate the car-bon intensity of PV power. Figure 3 gives an overview of SoLCAT's operation and utilization of data sources. Capacity refers to rated DC power capacity, unless otherwise indicated.

---

[2] The exact share depends on assumed electricity sources and other parameters, as elaborated in section 2.1.3.
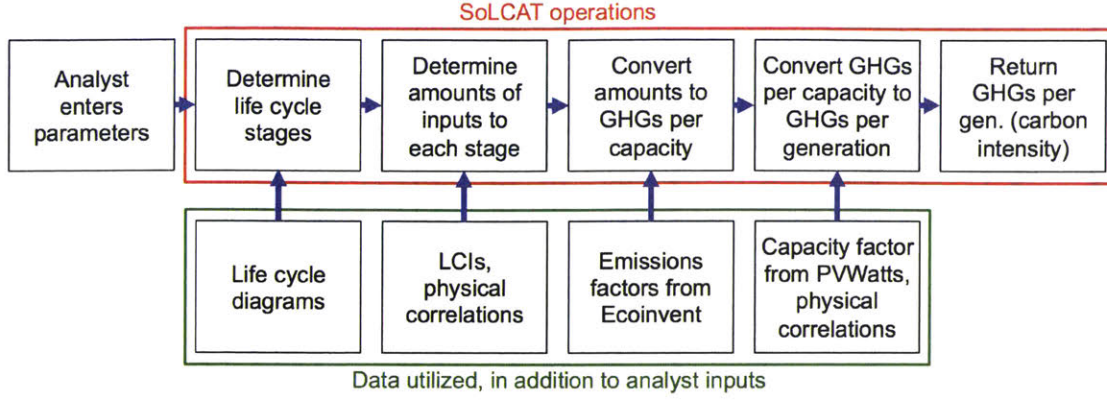
Figure 3. Flowchart of SoLCAT operations and utilization of data sources. Capacity is rated DC capacity. Generation is AC electricity generation.

SoLCAT converts amounts (a) to GHG emissions (e_{total}) using three general equations, shown below with indented examples after each equation:

$$e_{total} = \sum_i e_{stage\,i} \tag{1}$$

$$e_{total,mc-Si} = e_{Si-sand\,acquistion} + e_{MG-Si\,processing} \ldots + e_{cell\,prod.} \ldots + e_{installation} + e_{operation}$$

$$e_{stage\,i} = \sum_j e_{input\,j\,to\,stage\,i} - \sum_k^{stages\,before\,i} e_{stage\,k} \tag{2}$$

$$e_{MG-Si\,process.} = (e_{charcoal\,input\,to\,MG-Si\,process.} + e_{Si-sand\,input\,to\,MG-Si\,proc.} + \ldots) - e_{Si-sand\,acq.}$$

$$e_{input\,j\,to\,stage\,i} = a_{input\,j\,to\,stage\,i}\,EF_j \tag{3}$$

$$e_{chromium\,steel\,input\,to\,mounting\,prod.} = a_{chromium\,steel\,input\,to\,mounting\,prod.}\,EF_{chromium\,steel}$$

where e is emissions (g_C), a is amount (e.g., kg-iron, m^3-acetone, etc.), and EF is emission factor (e.g., g_C/kg-iron, g_C/m^3-acetone, etc.). Calculating life cycle emissions for one scenario involves >100 variations of equation (3) corresponding to different stages and inputs. Amounts ($a_{input\,j\,to\,stage\,i}$) are provided by the PV LCIs [29,47–49] or determined by input variables to SoLCAT. Emission factors (EF_j) are provided by Ecoinvent [47] or SoLCAT inputs. Table 2 describes how SoLCAT input variables impact amounts and emission factors.

Table 2
SoLCAT input variables and utilization by tool

Input variable [symbol] (unit)	Selectable values	Important uses in SoLCAT	Relevant equations (red indicates input variable)
Location of installation	locations across globe	Determines location inputs to: 1) PVWatts, which determines weather data (including irradiance, temperature, wind speed, and albedo) and thus effects year-one capacity factor; and 2) NREL's System Advisor Model snow model [54], which determines snow losses.	1) See section 2.1.4 and appendix on performance modeling. 2) $F_{snow} = F_{PVW}/(1 - f_{snow})$
Cell type	sc-Si mc-Si CdTe CIGS	1) Determines which module production LCIs are referenced and thus types and amounts of inputs to module production stages. (For mc-Si, an additional choice is made between Chinese and European production). 2) Determines cell type input to PVWatts, and thus thermal coefficient (γ) and other properties used to model performance. 3) If CdTe selected, adjusts nameplate error and light-induced degradation to 0% from PVWatts c-Si-based defaults of 1% and 1.5%, respectively	1) Eq. (3) 2) See section 2.1.4 and appendix Table A.1.
Installation type	utility, fixed tilt utility, 1-axis tracking rooftop, optimal tilt rooftop, typical tilt	1) Determines BOS LCIs referenced and thus types and amounts of inputs to BOS production stages (production of mounting, inverter & electrics) 2) Determines installation type and orientation input to PVWatts, which effects incident irradiance, module temperature, and year-one capacity factor. 3) Adjusts capacity factor for small tracker energy consumption based on [29]. If tracking not selected, $P_{track,perA} = 0$. i is irradiance (kWh/m²/yr).	1) Eq. (3) 2) See section 2.1.4 and appendix. 3) $F = \bar{F} - \dfrac{P_{track}}{c_{DC}} = \bar{F} - \dfrac{P_{track,perA}}{\eta_{STC} \times i_{STC}}$
Shading losses [f_{sh}] (fraction)	(continuous)	Adjusts capacity factor from PVWatts default shading to input shading.	$F_{yr\,1} = F_{snow} \times (1 - f_{sh})/(1 - f_{sh,pvw})$
Lifetime [t] (yr)	(continuous)	1) Adjusts capacity factor from year-one to lifetime average value. 2) Determines PV module area replaced due to operating damages.	1) $\bar{F} = F_{yr\,1} \times (1 - d \times t/2)$ 2) $A_{loss,op} = A_{op} \times f_{loss,op,1\,yr} \times t$
Efficiency, STC rated [η_{STC}] (fraction)	(continuous)	1) Determines PV module area required for installation of known DC capacity, not including installation and operating losses. 2) Determines mass of mounting system.	1) $A_{op} = c_{DC}/(i_{STC} \times \eta_{STC})$ 2) $m_{mount} = m_{mount\,per\,A} \times A_{op}$ $= m_{mount\,per\,A} \times c_{DC}/(i_{STC} \times \eta_{STC})$
Degradation rate [d] (fraction/yr)	(continuous)	Adjusts capacity factor from year-one to lifetime average value.	$\bar{F} = F_{yr\,1} \times (1 - d \times t/2)$
Inverter loading ratio [ILR] (ratio)	(continuous)	1) Determines inverter AC capacity required for installation of known DC capacity. 2) Impacts inverter efficiency and possibility of "clipping".	1) $c_{AC,inv} = c_{DC}/ILR$ 2) See section 2.1.4 and appendix Table A.3.
Upstream electricity emissions: module (gCO₂/kWh)	(continuous)	Provides emission factors of electricity used in module production stages.	Eq. (3)
Upstream electricity emissions: BOS (gCO₂/kWh)	(continuous)	Provides emission factors of electricity used in BOS production stages.	Eq. (3)
Shipping dist. from module prod. to installation (km)	(continuous)	Determines amount of shipping input to installation stage.	Eq. (3)
If mc-Si, module prod. typical of:	Europe China	Determines LCIs referenced for stages of mc-Si module production.	Eq. (3)

2.1.4. PV LCA - Converting GHGs per capacity to GHGs per generation (carbon intensity)

SoLCAT's last operation requires a capacity factor, or equivalently an energy yield. In estimating this factor, our methodology differs from that of prior multi-location PV LCAs [9,22,31], which treat performance ratio as temperature- and location-independent, and model AC electricity production as:

$$E_{AC} = A \times \bar{I} \times \eta_{STC} \times PR \times t \qquad (4)$$

where E_{AC} is AC electricity produced (kWh), A is module area (m^2), $\bar{I}$ is average solar irradiance (kW/m^2 or kWh/yr/m^2), η_{STC} is rated module efficiency, PR is performance ratio, and t is system lifetime (yr). Equation (4) is not used here because it limits what can be analyzed and is not the state of the art. More accurate and validated performance models are publicly available, and require negligible additonal computation. Our model utilizes capacity factor estimates from PVWatts [24]. PVWatts outputs year-one DC capacity factor based on inputs of: location, installation type, orientation, cell type, inverter loading ratio, rated inverter efficiency, ground coverage ratio, and system losses. To elaborate its role in our model and to underline important differences from equation (4), an outline of PVWatts' performance model is provided in the appendix.

As shown in Table 2, our model adjusts capacity factors from PVWatts to account for shading, snow, light-induced degradation (LID), non-LID degradation (commonly called "degradation"), and tracker energy consumption, to calculate a lifetime average capacity factor (F). Finally, carbon intensity is calculated as:

$$I = e_{total} / (F \times t_{hr}) \qquad (5)$$

where I is carbon intensity (g$_C$/kWh), e_{total} is life cycle GHG emissions per capacity (g$_C$/kW), and t_{hr} is PV system lifetime (hr).

Important differences between PVWatts' performance model and equation (4), and therefore between this work and prior PV LCAs, include: (1) module operating efficiency is modeled and temperature-dependent (see Table A.1), which enables more accurate modeling of power output across regions with significant temperature differences; (2) the interaction of location, orientation, and incident irradiance is

rigorously modeled (see Table A.2), which enables more accurate modeling of solar tracking's impact on power output in different locations; and (3) inverter efficiency is modeled and power-dependent (see Table A.3), which enables more accurate modelling of PV power output across different inverter loading ratios. In summary, PVWatts serves our goal of estimating PV power's carbon intensity under diverse conditions, by more accurately modeling the production of PV LCA's functional unit, AC electricity.

2.1.5. PV LCA - Tracking energy gain methodology

Analysis of solar tracking's impact on carbon intensity requires the calculation of tracking energy gain (TEG). TEG is the percent increase in PV power output that results from tracking the sun, relative to a fixed-position system, and can be estimated using PVWatts and equations (A.1) and (5) as

$$TEG = \left(\bar{P}_{AC,track} - \bar{P}_{AC,fixed}\right) / \bar{P}_{AC,fixed} \times 100\% \tag{6}$$

or equivalently

$$TEG = \left(F_{track} - F_{fixed}\right) / F_{fixed} \times 100\% \tag{7}$$

where F_{track} is the capacity factor of a PV system with tracking, and F_{fixed} is the capacity factor of a PV system with fixed orientation but otherwise identical features (location, modules, etc.). When discussing TEG, the details of both the tracking system (whether 1-axis or 2-axis, axis of rotation, rotation limits, etc.) and the fixed base case (tilt and azimuth) should be specified. In this thesis, the fixed base case orientation is always irradiance-maximizing, with equator-facing azimuth (south in northern hemisphere, north in southern hemisphere) and near-latitude tilt.

2.2. Model of combined generation and storage

2.2.1. Combined generation and storage - model of electricity supply to grid

Figure 4 shows an example of a generation curve (yellow) and a supply curve (blue). The generation curve shows how much electric power the generator is producing, while the supply curve shows how much power is supplied to the grid. When supply exceeds generation, the difference comes from storage, and when generation exceeds supply, the difference goes to storage. In Figure 4, typical variable PV gen-

eration is converted to constant supply. This is a simple example to illustrate the model. Infinite shapes are possible for the two curves, as long as the area under the supply curve does not exceed the area under the generation curve. The area under the supply curve will always be less than the area under the generation curve due to round-trip efficiency losses in storage. In Figure 4, P_0 is power generation (kW), P is power supply to grid (kW), $P_{s,in}$ is the amount of power generation sent to storage (kW), s is the instantaneous fraction of power generation going to storage, and $P_{s,out}$ is the power supply to grid from storage.
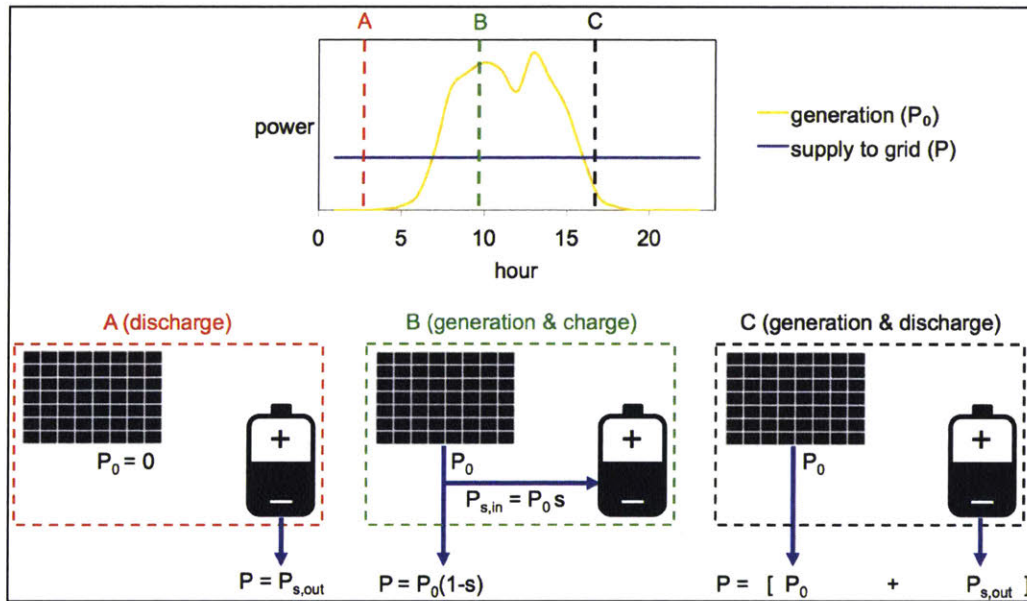

Figure 4. 3 scenarios corresponding to 3 times of day for a combined PV and storage system. P_0 is power generation (kW), P is power supply to grid (kW), $P_{s,in}$ is the amount of power generation sent to storage (kW), s is the instantaneous fraction of power generation going to storage, and $P_{s,out}$ is the power supply to grid from storage.

Averaging the power flows in Figure 4 produces Figure 5, which shows how the average power to grid can be calculated as

$$\bar{P} = \bar{P}_0[1 - f(1 - \eta)]$$

where η is the round-trip efficiency of the storage, and f is the fraction of energy generation sent to storage (vs. directly to grid). f is the generation-weighted average of s ($<sP_0>/<P_0>$), not the time-average ($<s>$). Lifetime electricity to grid can then be calculated as

$$E = t\bar{P} = t\bar{P}_0[1 - f(1 - \eta)] = E_0[1 - f(1 - \eta)] \tag{8}$$
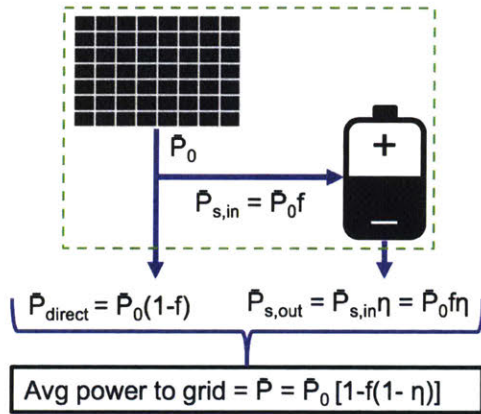

Figure 5. Average power flows of combined generation and storage. Over-bars indicate time averages, η is the round-trip efficiency of the storage, and f is the fraction of energy generation sent to storage (vs. directly to grid).

f depends on the generation and supply curves. Figure 6 illustrates this dependence, as well as how f changes with the degree of peak-smoothing.
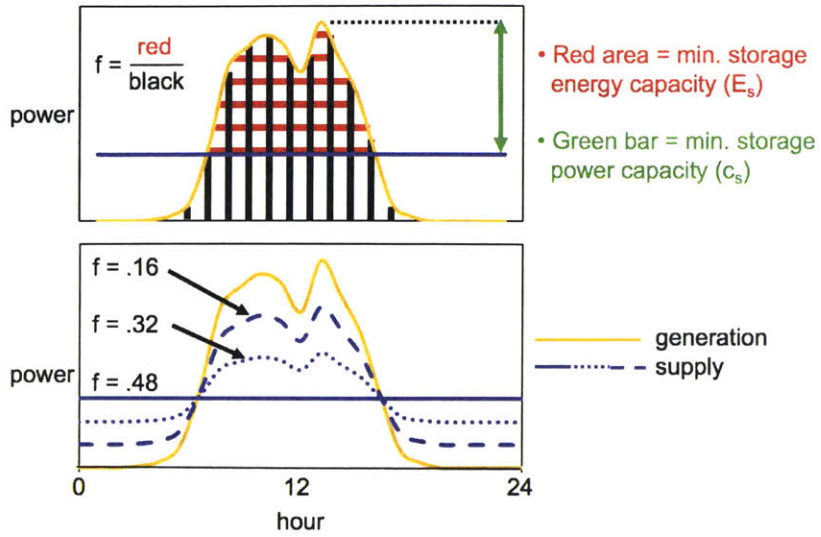

Figure 6. Dependence of f (fraction of generation sent to storage) on power generation and supply curves. Assumes no curtailment.

Figure 6 shows the minimum storage energy capacity and power capacity needed to convert the given generation to the desired supply. This thesis does not attempt to prescribe the optimum amounts of storage energy capacity, storage power capacity, or generation curtailment for a given desired f. For example, developers of a combined PV and storage plant that aims for constant supply must decide whether to install enough storage energy capacity to maintain supply to the grid for 3 or 4 or more consecutive cloudy days. These decisions involve risk-analysis and design choices that are beyond the scope of this thesis. This thesis provides tools to estimate how those different design choices impact emissions.

2.2.2. Combined generation and storage - model equations and parameters

Without storage, the emissions intensity I (g/kWh) of power generated and delivered to the grid can be calculated as

$$I_0 = e_g/E_0$$

where e_g is the life emissions of the generator (g), and E_0 is the life electricity generated (kWh). The subscripts 0 in I_0 and E_0 indicate the no-storage base case. In this thesis, the generator is assumed to operate nearly identically in the no-storage and storage-added cases, with the only difference being that, in the latter case, some of the generation is sent through storage on its way to the grid. In reality, the addition of storage to a power plant might change the way its generator is operated. For example, adding storage to a wind or gas power plant might enable reduced curtailment or increased fuel-to-power efficiency, respectively.

With storage in general and battery storage in particular, the emissions intensity of power delivered to the grid can be calculated (see section 2.2.3 for derivations) as, respectively,

$$I = [I_0 + f\eta(e_s/E_{sT})/(\bar{D}C)] / [1 - f(1 - \eta)] \tag{9}$$

and

$$I = [I_0 + f\eta(e_s/m_s)/(\rho\bar{D}C)] / [1 - f(1 - \eta)] \tag{10}$$

where f is the fraction of electricity generated that is stored (vs. sent directly to the grid), η is the round-trip efficiency of the storage, e_s is the life emissions of the storage (g), $\overline{D}$ is the average depth of discharge of the storage (DoD), E_{sT} is the total rated energy capacity of storage used over the power plant life (kWh), C is the cycle life of the storage (the number of charge-discharge cycles before a storage unit is retired), m_s is the mass of batteries used over the power plant life (kg), and ρ is the specific energy capacity of the batteries (kWh/kg). E_{sT} is the total rated energy capacity of all storage used and retired over the power plant life. For example, if the power plant storage system is rated at 1 MWh of energy capacity (E_s = 1 MWh), and 4 storage units are used and retired over the plant lifetime, then E_{sT} is 4 MWh.

Parameters in equations (9) and (10) depend on both design and technology, as shown in Table 3. Table 4 shows the values and ranges used in our case study for combined generation and battery storage. The ranges for efficiency and cycle life reflect uncertainties and variety in battery technologies. The purpose of this thesis, with regard to storage, is to provide an exploitable model for modeling emissions from combined generation and storage, and to demonstrate the use of that model given realistic literature-supported parameter ranges. Narrowing these ranges further would improve the model and it's specificity, potentially via the incorporation of correlations between cycle life and DoD, temperature, and charge-discharge rate. Such correlations can be found in [55] and [56]. This is one possible focus of future work. Battery production can be elaborated as shown in Figure 7. As with generation, this analysis does not consider end of life for storage.

Table 3.
Parameters in model equations and examples of dependencies. No example does not mean no dependence.

Symbol	Description	Units	Example of dependence on technology	Example of dependence on design
I_0	emissions intensity of electricity w/o storage	g/kWh	Coal gen. has higher GHG emissions than wind gen.	
f	fraction of electricity generation that is stored			Greater smoothing of generation peaks requires greater f. See Figure 6.
η	round-trip efficiency of storage		LBs usually have higher η than VFBs.	
e_s/E_{ST}	emissions per unit of rated storage energy capacity produced	g/kWh	Compared to LABs, LBs generally have higher GHG emissions per rated energy.	2 VFBs w/ same rated energy & different rated power will have different emissions.
e_s/m_s	emissions per unit of storage mass produced	g/kg		
ρ	specific energy capacity	kWh/kg		2 VFBs w/ same rated energy but different power will have different ρ.
$\bar{D}$	average depth of discharge (DoD)		LBs are usually run at higher DoD than LABs.	More "excess" storage energy capacity means lower D for same f.
C	cycle life	cycles	LBs have higher C than LABs.	

Table 4.
Parameter values in our case study of combined generation and battery storage. Values from Mitavachan [44].

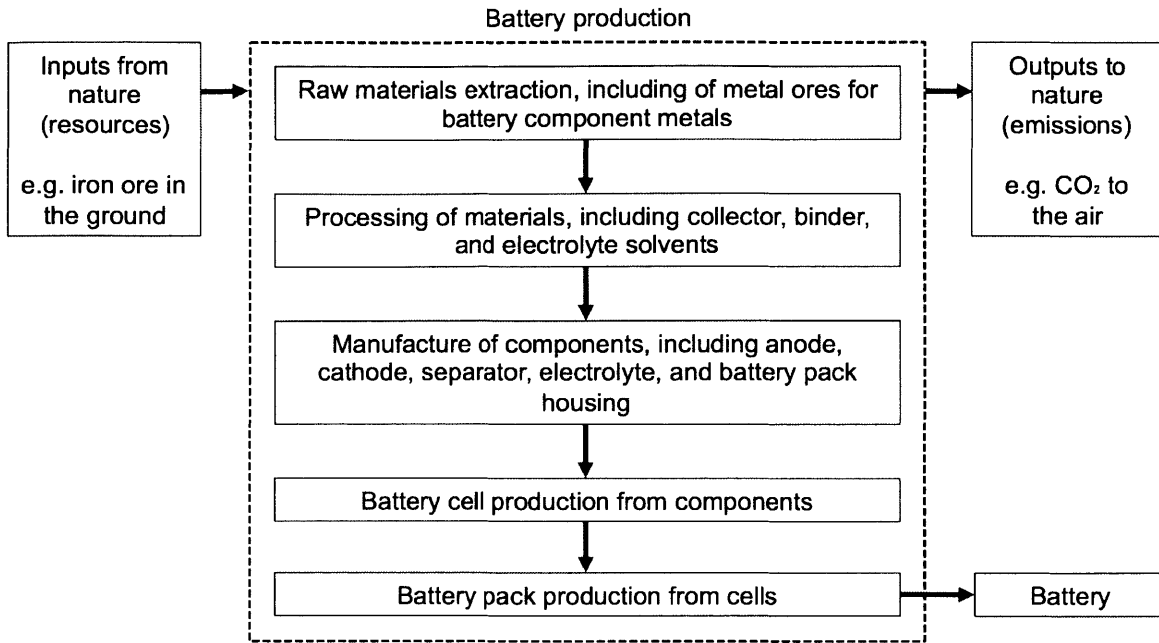|	η (%)			DoD	C (10³ cycles)			e_s/m_s (gc/g)	ρ (Wh/kg)
	avg	low	high		avg	low	high		
LB	90	85	98	0.8	10.25	5	15	22	140
VFB	75	60	80	0.9	13	10	15	2.7	20
LAB	82	80	90	0.8	1.25	1	1.5	2.7	27
SSB	81	71	90	0.8	13	10	15	14.9	116

Figure 7. Life cycle stages of battery production

The above equations apply not only to emissions (g) and emissions intensity (g/kWh), but also to any quantitative characteristic of both generation and storage. For example, the emissions values I_0 and e_s can be replaced with cost values to estimate the "cost intensity", i.e., the cost of electricity delivered to the grid from the combined generation and storage system ($/kWh).

2.2.3. Combined generation and storage - model equations derivations

The total number of storage charge-discharge cycles over a power plant's life can be calculated as

$$\#_{cyc} = E_{s,out}/E_{1cyc}$$

where $E_{s,out}$ is the total energy discharged from storage over the power plant's life (kWh), and E_{1cyc} is the average energy discharged per cycle (kWh). This equation can be expanded as

$$\#_{cyc} = \eta E_{s,in}/(\overline{D}E_s)$$

$$\#_{cyc} = \eta f E_0/(\overline{D}E_s) \tag{11}$$

where $E_{s,in}$ is the total energy sent to storage over the power plant's life (kWh), E_0 is the life electricity produced by the generator before storage (kWh); $\overline{D}$ is the average depth of discharge (DoD); and E_s is the rated energy capacity of the storage (kWh).

Let a "unit" refer to the rated storage system in place and operating at any given time. The number of units that "die" over the power plant's life can then be calculated as follows, if the storage unit reaches its cycle life before its calendar life:

$$\#_{deaths} = \#_{cyc}/C \rightarrow \text{plug in (11)}$$

$$\#_{deaths} = f\eta E_0/(\overline{D}CE_s) \tag{12}$$

where C is the cycle life and other variables are defined above. The total storage energy capacity used and retired over the power plant's life can then be calculated as

$$E_{sT} = \#_{deaths}E_s \rightarrow \text{plug in (12)}$$

$$E_{sT} = f\eta E_0/(\overline{D}C) \tag{13}$$

The life emissions of the storage can then be expanded as

$$e_s = e_s/E_{sT}\ E_{sT} \quad \rightarrow \text{plug in (13)}$$

$$e_s = e_s/E_{sT}\ f\eta E_0/(\bar{D}C) \tag{14}$$

$$e_s = e_s/m_s\ m_s/E_{sT}\ f\eta E_0/(\bar{D}C) \quad \rightarrow \text{if batteries, use definition of specific energy capacity}$$

$$e_s = e_s/m_s\ 1/\rho\ f\eta E_0/(\bar{D}C) \tag{15}$$

Finally, equation (14) or (15) can be plugged in to calculate the emissions intensity (g/kWh) of power delivered to the grid from a combined generation and storage system

$$I = (e_g + e_s)/E \quad \rightarrow \text{account for losses from storage (see Figure 5)}$$

$$= (e_g + e_s)/\{ E_0[1 - f(1 - \eta)] \}$$

$$= (I_0 + e_s/E_0)/[1 - f(1 - \eta)] \quad \rightarrow \text{plug in (14) or (15)}$$

$$I = [I_0 + f\eta(e_s/E_{sT})/(\bar{D}C)] / [1 - f(1 - \eta)] \tag{9}$$

and

$$I = [I_0 + f\eta(e_s/m_s)/(\rho\bar{D}C)] / [1 - f(1 - \eta)] \tag{10}$$

2.2.4. Combined generation and storage - Model assumptions and approximations include:

1) Storage efficiency is treated as constant.

2) The number of storage units retired over the system lifetime is treated as continuous in the model (see Eq. (12)).

3) In Table 2, the battery production emissions (e_s) do not include emissions from producing the battery inverter and control system, due to lack of data. An alternative is estimating battery inverter emissions by approximating that the battery inverters are equivalent to PV inverters and then using the PV inventories discussed in section 2.1.2. [48,49]. These inventories report inverter production GHGs of ~27.4 g_C per watt of AC inverter capacity, and inverter lifetime as 15 years. For the cases analyzed in this thesis, this would add approximately 1.5 g_C/kWh to total carbon intensity, and increase the storage production emissions by ~15% for LBs and ~30% for VFBs. Unlike the battery inverter case, we do not identify a reasonable approximation for emissions from producing the battery control system.

4) Charging from the grid is not analyzed. Such analysis would include expansion of the generator definition to encompass all generators connected to a grid.

5) Cycle life is considered controlling, not calendar life. Our analysis is focused on storage applications that require regular cycling at high DoD and thus cause cycling-induced degradation to be the primary degradation mode. The storage unit is assumed to reach its cycle life before its calendar life. For applications that do not involve high-use of battery capacity, such as frequency regulation, this might not be a valid approximation [44].

6) Temperature-induced degradation is not considered. More information on battery degradation modes can be found in [55] and [56].

7) DC-DC coupling is possible for PV and battery storage but not analyzed here. It is unclear whether DC-DC coupling of PV and batteries actually increases round-trip efficiency, given the particular equipment and system architecture required. For more discussion see [57].

8) Possible storage impacts on curtailment and generator efficiency are not analyzed. For example, storage can be used to store off-peak wind generation that would otherwise be curtailed, for later supply to grid. Thus, in some cases storage might actually increase the generator capacity factor F by offsetting storage efficiency losses with curtailment reductions. For another example, storage can be used to increase the fuel-to-power efficiency of simple cycle gas turbines (SCGT). A preliminary analysis suggests that, for an SCGT with an original generation profile typical of California peaker plants, adding enough storage to allow flat generation might increase generation-averaged fuel-to-power efficiency by up to ~3%, thus partly offsetting efficiency losses in storage.

2.2.5. Life cycle assessments of generation

A shown in equations (9) & (10), calculating emissions intensity requires knowing both the emissions from producing a unit mass of storage, and the emissions of generation without storage. GHG emissions per storage mass are given in Table 4. GHG emissions from combined-cycle gas and coal-fired generation have been estimated at 488 and 965 g_C/kWh, respectively [19]. For our case studies on combined renewa-

bles and batteries, we conducted an LCA of solar PV generation in section 2.1, and synthesize prior LCAs of wind generation in section 2.3.

2.3. Wind LCA synthesis

Wind electricity production can be elaborated as shown in Figure 8. To be consistent with our PV LCA, our wind system likewise excludes EOL and transmission from generation site to end-use.
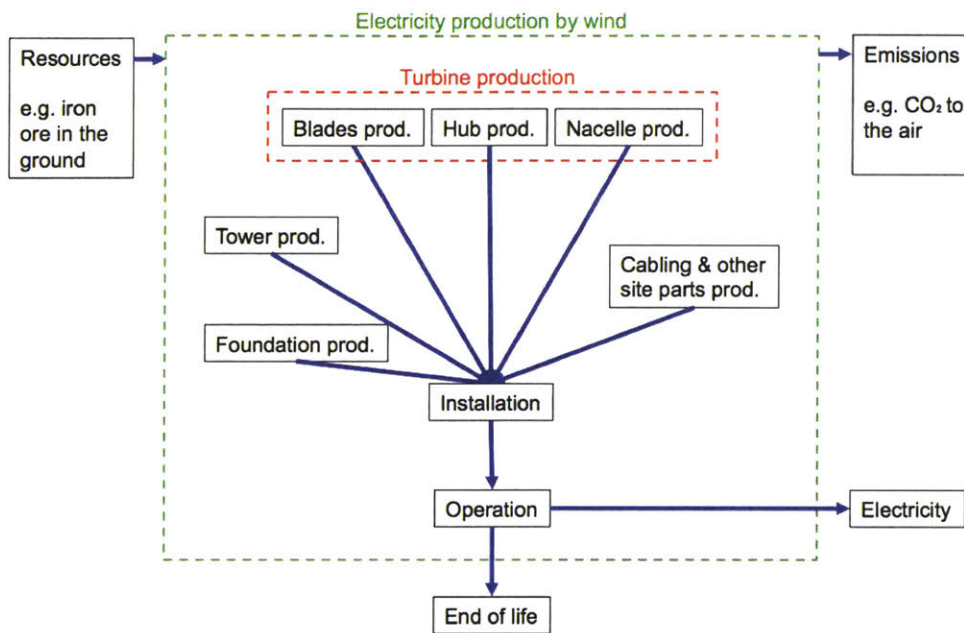

Figure 8. Life cycle stages of wind electricity production.

Our main data sources are 10 wind power LCAs conducted by the turbine manufacturers Vestas and Siemens-Gamesa (also called SWP) in 2011-2017 [10–17,58,59]. Vestas and SWP together accounted for ~25% and ~50% of new turbines installed in the world and US, respectively, in 2016 [7,60]. SWP accounted for over half of both cumulative and new offshore installations in 2016 [7]. These LCAs have been reviewed for compliance with ISO 14040 LCA standards, by external reviewers in Vestas' case and internal reviewers in SWP's case. The 10 turbine types modeled are widely deployed in conditions matching our 4 categories of interest: onshore low wind speed (~7m/s), onshore medium (~8m/s), onshore high (~9m/s), and offshore high (~9m/s). In the US, 4 of the 10 models are deployed in onshore low wind

speed conditions, 7 in onshore medium speed conditions, and 5 in onshore high speed conditions [8]. In

Europe, 3 of 10 are deployed in offshore high speed conditions [16,17,61].

Each LCA estimates the carbon intensity of generation from a "typical" wind farm of turbines of the

modeled type. The definition of "typical" varies slightly across the 10 LCAs. Thus, before averaging the

emissions figures in each of the 4 categories, we first harmonize several parameters. For example, we

assume a distance to grid of 20km for onshore wind farms [11]. If one LCA assumes 15km to grid and

emissions from grid cable production of 1 g_c/kWh, we multiply those emissions by 20km/15km = 1.33.

We also harmonize lifetime (20 years), hub height (95m), offshore distance to grid (70km [7]), and hourly

wind speed data (4 data sets for 4 categories). The wind speed data are input to NREL's System Advisor

Model program, along with the turbine model, to estimate capacity factors. Table 5 shows the results.

Table 5.
Carbon intensities of wind generation, from wind LCA synthesis [42-51].
(Assumptions include: onshore turbine size ~2MW, offshore turbine size ~5MW, onshore wind farm
20km from grid with 3% transmission losses (transmission just to grid), offshore wind farm 70km from
grid with 8% transmission losses, wind farm size >50MW, hub height 95m, wake losses 6%, availability
97%, offshore foundation monopile)

	Carbon intensity (gCO2e/kWh)		
	Avg	Low	High
Onshore high wind speed (~9m/s)	8.9	5.5	12
Onshore med wind speed (~8m/s)	9.7	6.4	12
Onshore low wind speed (~7m/s)	12	7.3	15.8
Offshore high wind speed (~9m/s)	14	10.8	18.2

3. Results and discussion

3.1. PV results and discussion

*Note: Some figure captions are long to accord with IEA PV LCA guidelines requesting system as-

sumptions be specified in captions adjacent to figures.*

SoLCAT results are compared here with the most up-to-date available results on life cycle GHG emis-

sions from mainstream PV power production, from Leccisi et al. [9]. Figure 9 shows good agreement

across cell types and irradiances. This is expected because both SoLCAT and Leccisi et al. use LCIs from the IEA's 2015 PVPS Report [49]. This agreement shows that our methodology can reproduce results obtained with a leader in LCA software programs, SimaPro, which is used by Leccisi et al. Small differences may be explained by uncertainties in exact grid emission factors assumed and by Leccisi et al.'s supplementation of the IEA LCIs with CdTe module and BOS LCIs that are not publicly available.
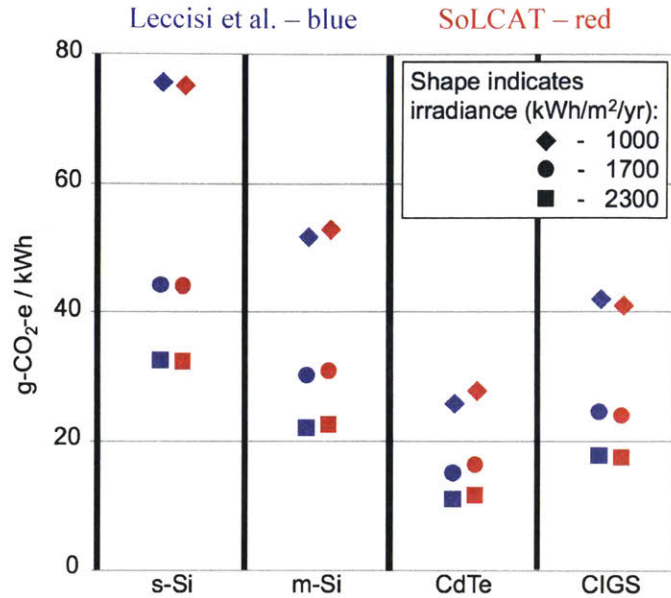
Figure 9. Carbon intensity of PV power by cell type and irradiance. Leccisi et al. [9] results are in blue, SoLCAT results in red. To correspond to Leccisi: mounting is open-ground fixed-tilt; lifetime is 30 years; rated module efficiencies are 17%, 16%, 15.6%, and 14%, left to right; performance ratio is a constant 0.8 across irradiances and accounts for shading and degradation, among other losses; US grid in 2015 is assumed for Si & CdTe modules, and Japan's grid in 2015 for CIGS modules, with US & Japan's grid GHG emissions set to 480 & 560 g_C/kWh, respectively, based on IEA electricity data [53]. Inverter loading ratio is assumed to be 1. Cell temperature and degradation are not specified by Leccisi et al., but must give a PR of 0.8 when combined with other losses. In SoLCAT, cell temperature and degradation are set at 25°C and 0.7%/yr, while other losses are adjusted to 9.5% to give PR = 0.8.

3.1.2. PV base cases and sensitivity analysis

Figure 10 shows how carbon intensity varies by location, irradiance, and cell type. The parameter values used in Figure 10 are assumed throughout the thesis unless otherwise indicated. Figure 11 shows the sensitivity of carbon intensity to two continous parameters, lifetime and degradation rate. An important non-continuous parameter is "production method". We find that, for Chinese mc-Si module production, using the "best technology" LCIs instead of the "mainstream" LCIs [49] produces a ~13% decrease in PV carbon intensity.
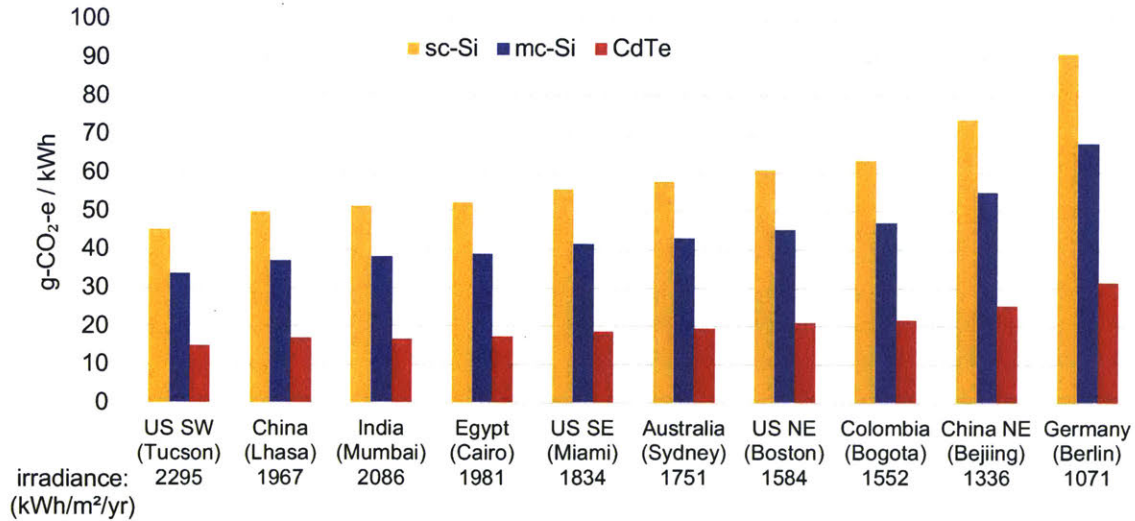
Figure 10. Base case carbon intensities of PV power from systems installed in different locations circa 2015. Installation type is large-scale (AC capacity >1MW), open-ground, fixed-tilt. Orientation is irradiance-maximizing. Irradiance is lifetime-average irradiance incident on modules. Lifetime is 30 years. Rated module efficiencies are 17%, 16%, and 15.6% for sc-Si, mc-Si, and CdTe, respectively, corresponding to average commericial efficiencies in 2015 [9]. Degradation is 0.7%/yr, corresponding to IEA PV LCA guidelines [23] and to measured degradation rates [33], which do not evidence a lower rate for CdTe vs. c-Si, despite warranties suggesting otherwise. Inverter loading ratio is 1. GHG emissions of upstream electricity are 660 gCOe/kWh for module production and 510 for BOS production, corresponding to Chinese & global averages in 2015 [53]. Total non-modeled losses, enumerated in methodology, are 14% for silicon and 11% for CdTe, due to differences in light-induced degradation and rating accuracy. These base case parameter values are assumed throughout the thesis unless otherwise indicated.
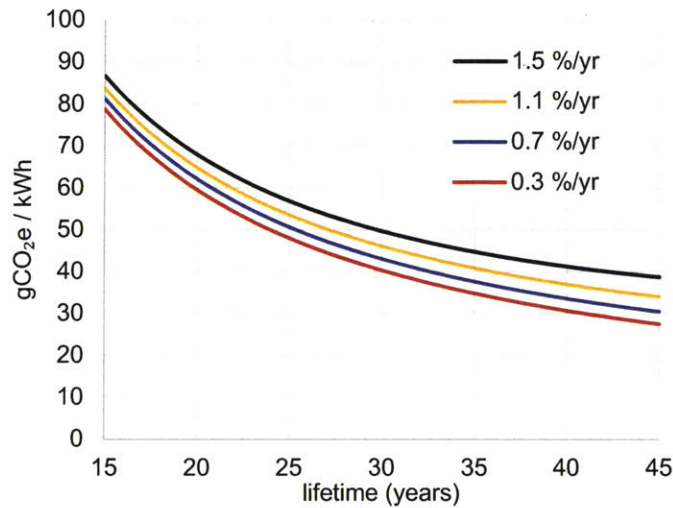

Figure 11. Carbon intensity of PV power vs. lifetime at different degradation rates. Installation location is Sydney, Australia. Cell type is mc-Si. Rated module efficiency is 16%. Other parameters match base case values in Figure 10.

Like EOL processes, PV system lifetimes are highly uncertain because the large majority of installed PV capacity (97%) has been operating for under 10 years [3]. The 30 year lifetime assumed in most PV LCAs is based loosely on module warranties, not on physical limits. After 30 years, a PV system with typical 0.7% degradation per year will still be generating 78% of its day-one power output at small operating cost, and thus might not be voluntarily shut down by its owner. Given the large uncertainties in lifetime, Figure 11 shows how PV carbon intensity varies over a range of liftetimes from 50% to 150% of the LCA-standard 30 years.

In contrast to lifetime uncertainty, uncertainties in rated efficiency, degradation, and weather can be approximately quantified based on empirical data, as shown by examples in Table 6. The numbers in Table 6 are meant to give approximate indicators of uncertainty and are not rigorous statistical measures. The last row follows NREL's recommendation to use weather data from multiple locations near the analyzed site to estimate uncertainties in energy production resulting from uncertainties in weather [62].

Table 6
Examples of uncertainty in parameters that impact the carbon intensity of PV power.

Variable	Typical uncertainty (corresponding ranges)	Based on:	Impact on PV carbon intensity: $\lvert(CI_{high} - CI_{low})\rvert / CI_{low} \times 100\%$
Rated efficiency of mc-Si modules purchased from a single product line and installed at a site	1% absolute (16 - 17 %)	Specification sheets of 20 mc-Si product lines being sold by the top 3 Chinese module manufacturers in 2018 [63–65]. A single product line's spec sheet does not give a discrete rated efficiency, but rather a range, and for these 20 lines, that range is typically ~1% absolute.	5%
Degradation rate of c-Si PV modules installed at a site	0.3 %/yr (0.9 – 1.2 %/yr)	The 95% confidence interval for measured degradation rates of 68 c-Si modules tested at 5 sites in western India in the "hot & dry" climate category [34]. "Hot & dry" sites are defined in the survey as having ≥ 6 months with mean temperature over 30 °C and humidity under 55%, respectively. See section 3.1.3 for more detail on this survey.	10%
Lifetime avg. weather at a location	Irradiance in kWh/m²/yr: Δ_{mean} ~ 47 (1000-1047, 2000-2047) Δ_{95} ~ 120 (1000-1120, 2000-2120) temperature: Δ_{mean} ~ 0.6 °C (10-10.6 °C, 20-20.6 °C) Δ_{95} ~ 1.5 °C (10-11.5 °C, 20-21.5 °C)	Irradiance and temperature differences across 30 pairs of locations, with each location-pair in the same US municipality. For example, 1 data-point is the recorded average irradiance difference between east & west Houston. Each location pair has a latitude difference under 0.2°. Data is from "TMY3" files in the National Solar Radiation Database [62]. Δ_{95} ~ 120 kWh/m²/yr indicates that ~95% of these location-pairs have irradiance differences under 120 kWh/m²/yr. Irradiance is GHI.	2.5 - 4% for means 6 - 10% for 95-values

3.1.3. PV temperature impacts

Inter-regional temperature variations can have a significant impact on the carbon intensity of PV power. As a case study, this thesis analyzes two hypothetical identical open-ground mc-Si PV systems, one in the US northeast (Boston, Massachusetts) and one in the US southwest (Phoenix, Arizona). Using the equations in Tables A.1-A.3, cell temperature and module efficiency are calculated for a meteorologically average March day and plotted in Figure 12.
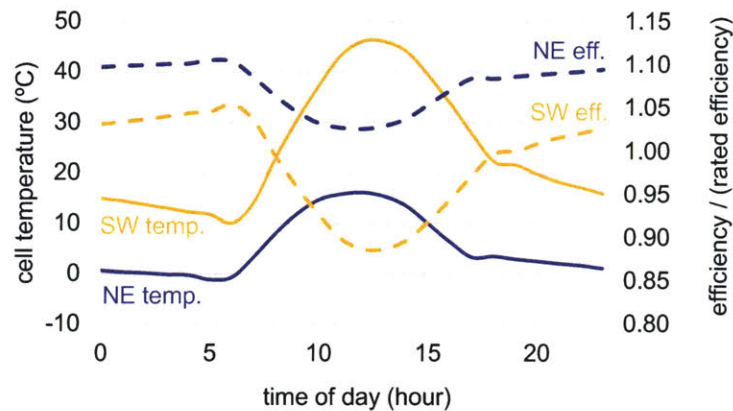

Figure 12. Cell temperature (temp.) and operating efficiency (eff.) of mc-Si PV modules in the US northeast (NE, Boston) and the US southwest (SW, Phoenix) on an average March day, calculated using the PVWatts performance model outlined in Tables A.1-A.3. Averaging over the month smooths out hour-to-hour fluctuations. The weather data used are "Typical Meteorological Year" (TMY2) weather files used by PVWatts, with hourly data for 12 months. Each month is from a specific year, and which month comes from which year is determined by statistical methods to best represent a multi-year period. More information on TMY weather data can be found in [62].

Across all months, the generation-averaged cell temperature is 24.5 °C in Boston and 45.3 °C in Phoenix.[3] As a result, the modules' average year-one operating efficiency is 10% lower in Phoenix than in Boston (14.3% vs. 15.8%). Assuming operating efficiency and performance ratio independent of temperature, as has been typically done in PV LCA, would be equivalent to holding cell temperature constant at 25°C or setting the thermal coefficient (γ) to 0 %/°C in Table A.1. Doing so would negligibly change the estimated power output of the Boston system (<0.1% change), but would overestimate the power of the Phoenix

---

[3] "Average" in this section (3.1.3) means generation-averaged. Generation-averaged efficiency is the average efficiency at which electricity is generated. Time-averaged module efficiency is less relevant, because it weights nighttime and cloudy-skies efficiency the same as day-time and clear-skies efficiency.

system by 11%, and thereby underestimate PV carbon intensity by 13% (31 vs. 35 g$_C$/kWh).[6] Similar analyses can be applied to other regions, as shown in Figure 13. In each of the warm locations, neglecting reversible temperature impacts on module efficiency leads to underestimates of the carbon intensity of silicon PV power (by 9% in Singapore, 10% in the US southwest, 11% in western Mexico, and 13% in western India).
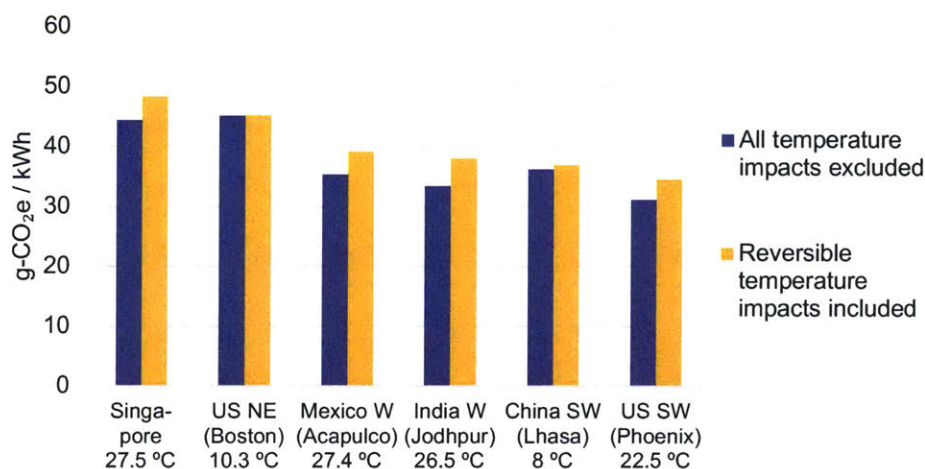

Figure 13. Carbon intensity of mc-Si PV power in select regions. Mean ambient temperatures are at bottom. "Reversible temperature impacts included" (yellow) utilizes the full performance model outlined in methodology and the Sappendix. "All temperature impacts excluded" (blue) utilizes the same model, except with cell temperature held constant at 25°C for all locations and times, and PR constant at 0.80, except for Boston which has PR of 0.79 due to snow losses). Note how excluding temperature impacts (blue) disturbs the monotonic decrease in carbon intensity left to right. Consistent with the base case, degradation of 0.7 %/yr is assumed for all. Temperature-dependent degradation is discussed later.

Figure 13 illustrates the reversible impacts of temperature on module efficiency. Irreversible impacts, i.e., temperature-induced degradation, can also be significant [33,34]. Modeling the complex modes of such impacts, including encapsulant discoloration, interconnect corrosion, and cell micro-cracking, is

---

[4] Due to uncertainties described in Section 3.1, this thesis reports carbon intensity to 2 significant figures. As a result, in a few cases, reported carbon intensities and reported percent difference might seem inconsistent, but are not. For example, if emissions for Scenarios A & B are computed as 19.3 & 20.7 g$_C$/kWh, they are reported as 19 & 21 g$_C$/kWh. To compute the percent difference, non-rounded numbers are always used in intermediate calculations. Thus, Scenario B emissions are computed to be 7% higher than Scenario A emissions, because $(20.7 - 19.3)/19.3 = .07$. If the rounded numbers were used for the intermediate calculation, the percent difference would be incorrectly computed as 11%, because $(21-19)/19 = .11$.

beyond the scope of this thesis. However, these effects can be very approximately accounted for based on empirical degradation rates. The 2014 and 2016 "All-India Surveys of PV Module Reliability" [34] found statistically significant differences in irreversible degradation between "hot" and "cold" climates of 0.96 %/yr (1.18 vs. 0.24 %/yr), based on 251 modules tested at 22 "hot" sites, and 126 modules tested at 5 "cold" sites. "Hot" sites had mean annual temperatures above 22 °C and were located in western, southern, and central India, while "cold" sites had temperatures below 12 °C and were located in northern India. This degradation difference means that the "hot" modules' power output typically declines by ~35% over 30 years, while the "cold" modules' output declines by ~12%. These numbers likely give a conservative estimate of the temperature-dependent degradation difference between climates because the survey excluded sites with mean degradation over 2 %/yr, which filtered out 6 of 28 "hot" sites, but only 0 of 5 "cold" sites.

As a case study of irreversible temperature effects on PV carbon intensity, we analyze two hypothetical mc-Si PV systems at two sites covered in the report, Chennai in southern India and Srinagar in northern India. Figure 14 shows that accounting for temperature impacts significantly alters the inter-regional emissions comparison. If performance ratio is assumed constant between regions (blue bars), mc-Si PV power in northern India is estimated to be 21% more carbon intensive than in southern India (42 vs. 35 g_C/kWh). If reversible temperature effects are accounted for (yellow bars), the estimated gap shrinks to 13% (44 vs. 39 g_C/kWh). And if all temperature effects are accounted for (red bars), we estimate that mc-Si PV power in northern India is 5% *less* carbon intensive than in southern India (41 vs. 43 g_C/kWh). The adjustment from blue to yellow is based on reversible temperature-driven efficiency changes that are well understood and based on thousands of tested modules [24]. The adjustment from yellow to red is based on empirical data on irreversible temperature-driven efficency losses, with causes that are not well modeled (e.g., interconnect corrosion). Thus the changes from yellow to red should be understood as a first-cut approximtion of how regional temperature differences can affect the emissions intensity of PV power via degradation.
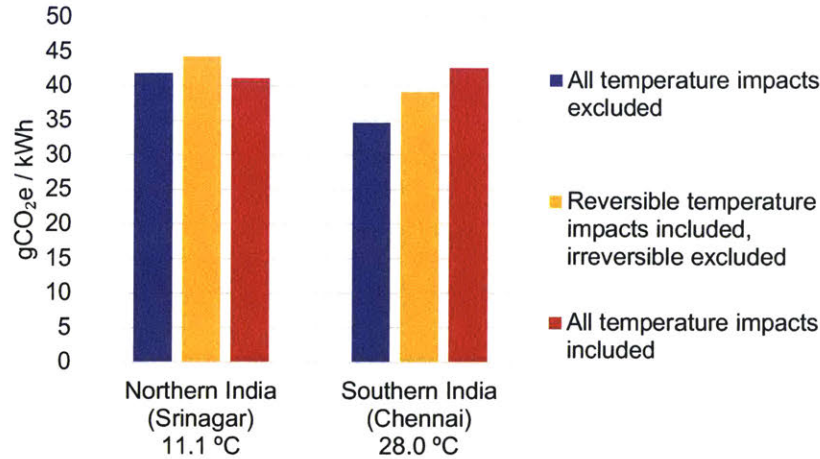
Figure 14. Carbon intensity of PV power from mc-Si systems in northern and southern India. Mean ambient temperatures are at bottom. "All temperature impacts included" (red) utilizes the full performance model outlined in methodology and appendix, and empirically based degradation rates from [34] of 0.24 and 1.18 %/yr in northern and southern India, respectively. "Reversible temperature impacts included, irreversible excluded" (yellow) utilizes the full model with variable temperature, and PV LCA-standard degradation of 0.7%/yr for both systems. "All temperature impacts excluded" (blue) utilizes the same model, except with cell temperature held constant at 25°C and PV LCA-standard degradation of 0.7%/yr for both systems. Colors are consistent with Figure 13.

The locations in Figures 10 and 11 are selected to demonstrate potential error in carbon intensity from ignoring temperature impacts. In some locations, this error will be negligible (e.g. in Boston the error is <0.1%). However, it will not be negligible in warm locations or when comparing PV across regions with significant temperature differences (>10 °C). Such temperature differences exist both between countries and within single large countries, including India, the US, and China. The analysis above is based on the denominator in carbon intensity, the kWh in g_C/kWh, and can thus be applied to emissions of other pollutants, not only GHGs.

3.1.4. PV inverter overloading

As commonly practiced (ILR <1.5), inverter overloading slightly diminishes the carbon intensity of PV power. As a case study, this thesis analyzes three hypothetical CdTe PV rooftop installations with ILRs of 1, 1.25, and 1.5, in the US state of North Carolina. These ILRs span the range seen generally in the US, and specifically at 40 CdTe projects operating in North Carolina in 2016, which had mean and

maximum ILRs of 1.29 and 1.47, respectively [8]. The results are shown in Figure 15. Increasing ILR from 1 to 1.5 reduces carbon intensity by 1.5 g_C/kWh (8%). Overloading the inverter with increased panel capacity can also be viewed as "underloading" the panels with decreased inverter capacity. That is, inverter overloading shrinks the inverter capacity required per module. This will of course reduce inverter production emissions (and cost) per module (see purple sections in Figure 15). If there is no reduction in power output per panel (i.e., no reduction in DC capacity factor), this will also reduce emissions per power (carbon intensity). An arguably counterintuitive result is: Adding 50% more modules to an existing PV installation with ILR of 1 slightly reduces the installation's carbon intensity. For silicon PV, the absolute change will be similar and the percent change smaller, due to silicon's greater module production emissions.
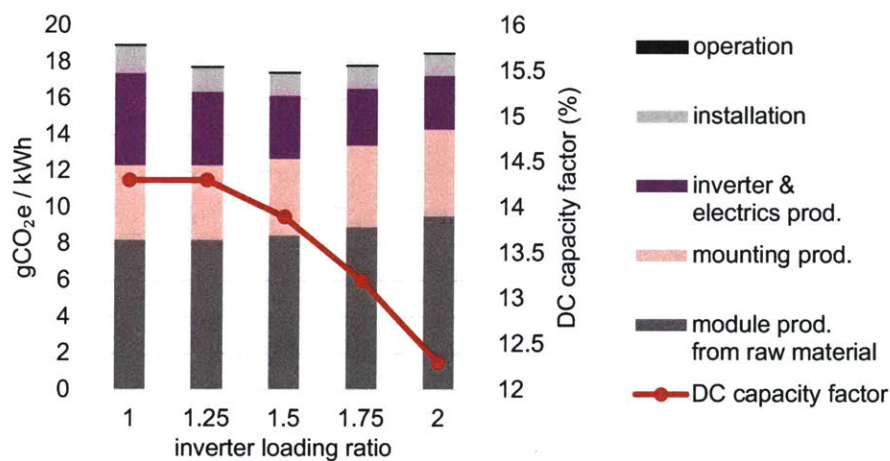

Figure 15. Carbon intensity (left axis) & capacity factor (right axis) of CdTe PV systems with inverter loading ratios between 1 and 2. Installation location is near Charlotte, North Carolina, US, and installation type is roof-mounted with optimal tilt. Other parameters values match base case in Figure 10. Carbon intensity drops as ILR rises from 1 to 1.5, due to reduced inverter material per module (see purple sections), and rises as ILR exceeds 1.5, due to reduced power output per module (see red line).

Increasing ILR further to 1.75, does not further reduce carbon intensity, due to "clipping". For a typical PV system with a self-limiting inverter, if its modules begin to generate DC power above the inverter's input capacity, the inverter "clips" the power by raising its voltage. Power that would be converted to AC if the inverter was bigger is instead never created. Clipping is rare for most PV systems without in-

---

[5] ILRs of 1.7 or more are currently rare but not unseen, having been installed at large-scale PV projects (AC capacity >1 MW) in at least 6 US states as of 2016 [8].

verter overloading, because modules at real-world installations rarely reach their rated DC power. However, at high enough ILRs, power clipping becomes significant, as shown by the capacity factors (red line in Figure 15) dropping at ILRs above 1.25. This drop in carbon intensity's denominator (kilowatthours of power output) offsets the continued drop in inverter emissions, such that carbon intensity rises as ILR exceeds 1.5.

3.1.5. PV solar tracking

We find that in the US southwest, for mc-Si PV, horizontal 1-axis tracking reduces carbon intensity by 12% relative to the fixed-tilt base case (from 34 to 30 g_C/kWh), consistent with previously published results [9]. Tracking produces this reduction despite requiring ~50% more structural metal (iron and aluminum) and ~30% more copper cable per module, compared to fixed-tilt mounting [29]. Emissions from producing the extra tracker materials (note the pink sections in Figure 16) are offset by increased generation from tracking, such that overall carbon intensity decreases.

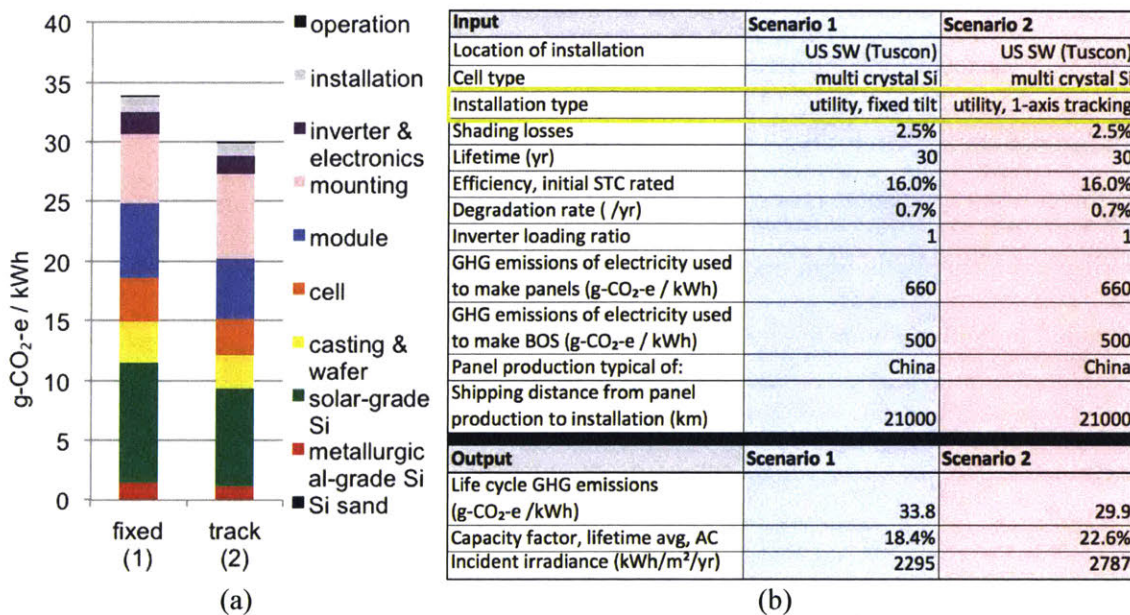| Input	Scenario 1	Scenario 2
Location of installation	US SW (Tuscon)	US SW (Tuscon)
Cell type	multi crystal Si	multi crystal Si
Installation type	utility, fixed tilt	utility, 1-axis tracking
Shading losses	2.5%	2.5%
Lifetime (yr)	30	30
Efficiency, initial STC rated	16.0%	16.0%
Degradation rate (/yr)	0.7%	0.7%
Inverter loading ratio	1	1
GHG emissions of electricity used to make panels (g-CO_2-e / kWh)	660	660
GHG emissions of electricity used to make BOS (g-CO_2-e / kWh)	500	500
Panel production typical of:	China	China
Shipping distance from panel production to installation (km)	21000	21000
Output	**Scenario 1**	**Scenario 2**
Life cycle GHG emissions (g-CO_2-e /kWh)	33.8	29.9
Capacity factor, lifetime avg, AC	18.4%	22.6%
Incident irradiance (kWh/m²/yr)	2295	2787

(a)   (b)

Figure 16. (a) Carbon intensity of fixed-tilt vs. tracking PV in US SW. (b) Corresponding inputs to SoL-CAT. To facilitate comparison with prior LCAs, ILR of 1 is used here, but it should be noted that ILR >1 is now the norm for new installations.

To determine if this ~10% emissions reduction holds for other regions and cell types, we apply analogous calculations to hypothetical mc-Si and CdTe PV systems at 10 other locations (the base cases from Figure 10) and present them in Figure 17, which underlines several related findings. (1) location influences the emissions impact of tracking, via tracking energy gain (TEG); (2) tracking decreases the carbon intensity of mc-Si PV in most locations; (3) consistent with Sinha et al. [29], tracking reduces the carbon intensity of CdTe PV in the US southwest by ~3%; and (4) the US southwest is the exception to the rule: for most locations tested, tracking actually increases the carbon intensity of CdTe PV power. This includes many places with favorable economics for tracking and TEG above 13%. Near Sydney, Australia, for example, horizontal single-axis tracking increases both electricity output (by 14%) and carbon intensity (by 5%, from 19 to 20 g_C/kWh). In Germany, where tracking is less common, tracking increases power output by 6% and emissions by 13% (from 31 to 35 g_C/kWh).

The dependence on location is mainly driven by latitude and cloud cover. The greater the latitude, the greater the module tilt that maximizes incident irradiance, and the more irradiance is lost by "reclining" to a horizontal tilt for 1-axis tracking.[6] Greater latitude also means more atmosphere for sunlight to travel through. This increases light scattering, as does greater cloud cover. The greater the fraction of ambient light that is scattered (i.e., diffuse), the less energy there is to be gained from tracking the sun's non-diffuse direct beam irradiance. Lower tracking energy gain (TEG) means less extra electricity over which to amortize extra emissions from tracker-production. For both module types, this explains why, as TEG decreases left to right in Figure 17, tracking's emissions impact increases in relative terms (the bars).

---

[6] As described in section 1.2, horizontal 1-axis tracking is the norm for large-scale tracking. Tilted 1-axis trackers do exist, but are much less common for reasons including self-shading and wind concerns.
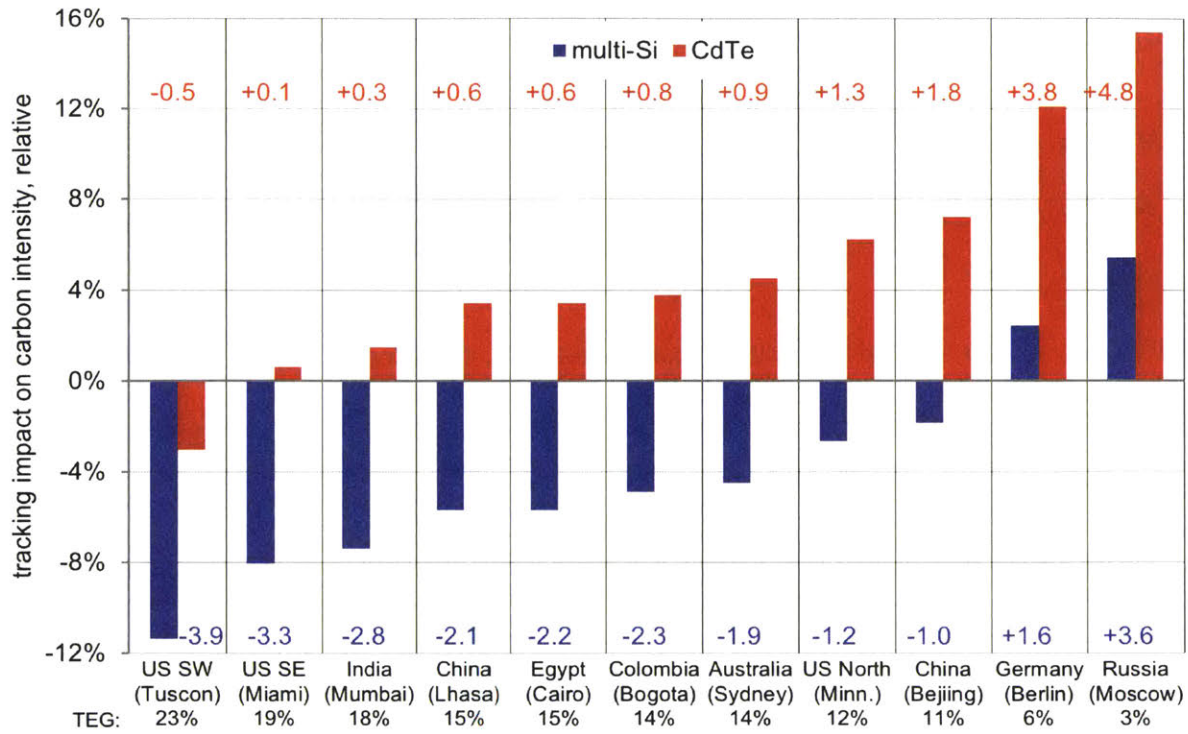
Figure 17. The impact of horizontal 1-axis solar tracking on PV carbon intensity in different locations, for mc-Si PV (blue), and CdTe PV (red). The y-axis and bars indicate relative impact, i.e., percent change in carbon intensity compared to fixed PV at the same location: %-change = $(CI_{tracking\ PV} - CI_{fixed\ PV})/$ $CI_{fixed\ PV} \times 100\%$. The red and blue numbers indicate absolute impact (g$_C$/kWh): absolute change = $(CI_{tracking\ PV} - CI_{fixed\ PV})$. Tracking energy gains (TEGs) are at bottom.

The varying impact by module type can be explained with the following equations:

Let: $T \equiv$ the factor by which tracking increases electricity generation. E.g., If TEG = 20%, $T = 1.2$.

$e_{f,i} \equiv$ emissions of fixed PV system (g$_C$). i = mc-Si or CdTe

$e_t \equiv$ emissions from adding tracking (g$_C$)

$E_f \equiv$ generation from fixed PV system (kWh)

$E_t \equiv$ generation from tracking PV system (kWh)

$I_f \equiv$ emissions per generation (carbon intensity) of fixed PV system (g$_C$/kWh)

$I_t \equiv$ emissions per generation (carbon intensity) of tracking PV system (g$_C$/kWh)

$M \equiv$ factor by which tracking changes carbon intensity. Figure 17 shows

$(M - 1) \times 100\%$, the percent by which tracking changes carbon intensity.

43

Using these definitions:

$$M = I_t / I_f$$

$$= [(e_{f,i} + e_t)/E_t] / [e_{f,i}/E_f]$$

$$= [(e_{f,i} + e_t)/(T \times E_f)] / [e_{f,i}/E_f]$$

$$M = (1 + e_t/e_{f,i})/ T \tag{18}$$

Only if $e_t/e_{f,i} <$ (T-1) will adding a tracker reduce emissions. Consider equation (18) when $e_{f,i} \gg e_t$, i.e., when emissions from module production are much larger than emissions from tracker production:

$$M_{f\ large} = 1/T \tag{19}$$

$M_{f\ large}$ will always be less than 1, because T is always greater than 1. In other words, for a module type with large production emissions, adding tracking will reduce carbon intensity. This explains why adding tracking reduces the carbon intensity of mc-Si PV in most locations (blue bars in Figure 17). Multi-Si module production is significantly more carbon intensive than CdTe module production, as seen in Figure 2 and previously reported [49]. $e_{f,multi-Si}$ is approximately 11 × e_t, whereas $e_{f,CdTe}$ is approximately 5 × e_t. Equation (18) thus also explains why adding tracking increases CdTe PV's carbon intensity in most locations (red bars in Figure 17):

$$M_{CdTe} = [1 + e_t/e_{f,CdTe}]/ T$$

$$\approx [1 + e_t/(5e_t)]/ T$$

$$M_{CdTe} \approx 1.2/T \tag{20}$$

For M_{CdTe} to be less than 1, T must be greater than 1.2. In other words, CdTe PV requires TEG above 20% for tracking to reduce its carbon intensity, a TEG only possible in exceptionally sunny regions like the US southwest.

Figure 18 illustrates the general principle behind both scenarios (high and low module emissions). In the future, if the ratio of module production emissions to tracker production emissions increases, independent of absolute emission values, tracking will more commonly decrease PV carbon intensity.
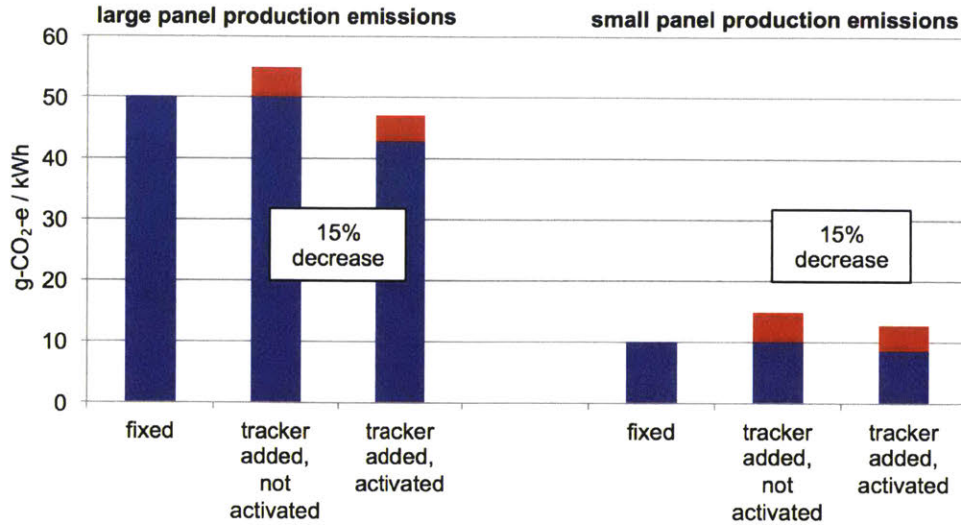
Figure 18. Illustration of how panel production emissions influence whether tracking decreases (left) or increases (right) carbon intensity, relative to fixed PV. Left and right systems have the same location and power output per panel. Activating tracking on both boosts power by 17%, a typical TEG for a sunny location. Red is the tracker contribution to emissions. In terms of equation (18) definitions, red represents e_t/g_f in the "not activated" bars, and e_t/g_t in the "activated" bars. Emissions values in this figure are arbitrary and chosen to illustrate the concept. TEG of 17% is assumed, giving a 15% reduction in carbon intensity upon activation.

Given that one claim of this thesis is that modern PV performance modeling can benefit PV LCA, it is relevant to point out that prior PV LCAs addressing tracking have made significant errors in estimating TEG. Bayod-Rújula et al. [25] accurately estimated 2-axis TEG in central Spain of 38%, but then generalized this number to Berlin, where in reality TEG will be at most 25%, due to greater latitude and diffuse light fraction. Beylot et al. [27] assumed an unrealistically low TEG of 5% for 1-axis tracking with 30° tilt, given annual irradiance of 1700 kWh/m²/yr on a 30°-tilted plane, at a hypothetical project of unspecified location. Desideri et al. [26] assumed a ~5-times-greater TEG of 26%, also for 1-axis tracking with 30° tilt and similar irradiance (1600-1800 kWh/m²/yr) at a hypothetical project near Gela, Sicily. For the conditions stated by Desideri et al., 26% TEG is significantly higher than the 20% TEG that PVWatts and equation (7) would estimate in Gela. This is due to the study's incorrect use of an AC power equation that assumes irradiance on a surface that is always normal to the sun's rays; however, 1-axis tracking cannot keep a module surface normal to the sun's rays, unlike 2-axis tracking. Using PVWatts and equation (7) to estimate TEG for a 2-axis tracking system in Gela gives a value of 25%, relative to a fixed PV system

facing south with 30° tilt, further suggesting that the authors calculated a 2-axis TEG for a 1-axis tracking system.

3.1.6. PV manufacturing location

A harmonization series provides insight into emissions differences between Chinese and European supply chains for mc-Si modules. Consider two scenarios in which mc-Si modules are installed at a utility PV site near Berlin, Germany. The hypothetical German installer has a choice of modules. In scenario 1 the modules are sourced from China; in scenario 2, from Germany. Inputs to SoLCAT are selected accordingly for production inventory, production grid emissions, and shipping distance from production to installation, as seen in Figure 19. Production grid emissions are based on 2015 IEA data on electricity emissions (470 and 660 g_C/kWh for Germany and China, respectively) [53], and shipping distance is based on the commercial ports nearest to production (Shanghai) and installation (Bremerhaven) [66].

Input	Scenario 1	Scenario 2
Location of installation	Germany (Berlin)	Germany (Berlin)
Cell type	multi crystal Si	multi crystal Si
Installation type	utility, fixed tilt	utility, fixed tilt
Shading losses	2.5%	2.5%
Lifetime (yr)	30	30
Efficiency, STC rated	16.0%	16.0%
Degradation rate (/yr)	0.7%	0.7%
Inverter loading ratio	1	1
GHG emissions of electricity used to make panels (g-CO_2-e / kWh)	660	470
GHG emissions of electricity used to make BOS (g-CO_2-e / kWh)	470	470
Panel prod. typical of:	China	Europe
Shipping distance from panel production to installation (km)	17300	300
Output, lifetime average	**Scenario 1**	**Scenario 2**
Life cycle GHG emissions (g-CO_2-e /kWh)	67.5	53.2
Capacity factor, DC	9.2%	9.2%
Incident irradiance (kWh/m²/yr)	1071	1071

Figure 19. GHG emissions (red box) of mc-Si PV installed in Germany and produced in China or Europe, and corresponding inputs to SoLCAT (differences in yellow box).

Under these conditions, the life cycle GHG emissions of the Chinese-produced modules are 27% higher (68 vs. 53 g_C/kWh). To explain this emissions gap, we utilize step-by-step harmonization. First we harmonize shipping distance to 17300 km in both scenarios, and second we harmonize GHG emissions of upstream electricity to 660 g_C/kWh in both scenarios. Figure 20(a) shows that (1) shipping contributions to the emissions difference are small (only 7% of the initial gap), and (2) electricity source determines a large part of the emissions difference (48%). That is, Chinese module production relies on grid electricity that is more carbon-intensive than European electricity. However, as the final harmonization shows, a nontrivial emissions gap remains, approximately half the original difference. In other words, even with identical shipping distances and electricity sources, the two regions' module supply chains are non-identical in emissions-relevant ways. Figure 20(b) shows how: Chinese module production not only uses electricity that is more carbon-intensive (more GHGs per input kWh); it also uses a greater *amount* of that electricity (more input kWh per module), and in addition, more fuel. The mainstream Chinese and Euro-pean LCIs [49] indicate that, across all module production stages (silica sand acquisition through module assembly in Figure 2), Chinese module production uses ~30% more electricity per module manufactured.
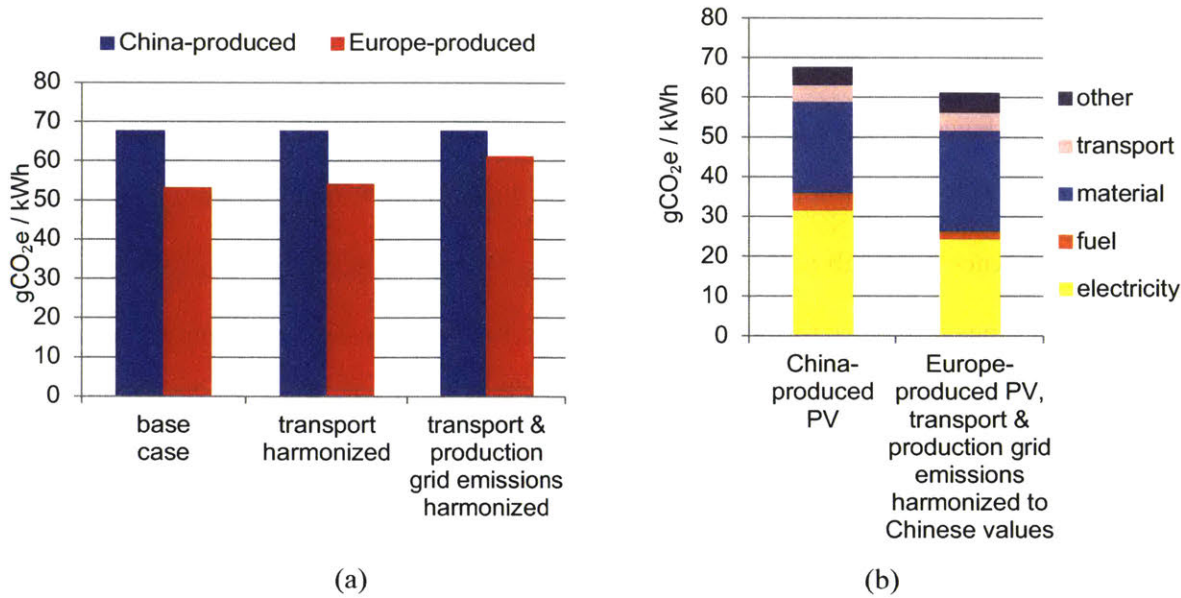
Figure 20. (a) Impact of harmonization on GHG emissions of mc-Si PV. Transport is harmonized by setting European panel shipping distance equal to Chinese value of 17300 km. Grid emissions are harmonized by setting European grid emissions equal to Chinese value of 660 g_C/kWh. (b) Emissions breakdown by category of input to foreground stages. Foreground refers to the life cycle stages in Figure 2. Note: foreground gives an approximate sense of stages controlled by companies in the PV supply chain. "Material" "transport" and "other" GHG emissions in the foreground can ultimately be traced back to carbon fuel use in the background (e.g. in steel production) in most cases.

3.2. Coupled generation and storage: results and discussion

3.2.1. Coupled generation and storage: results

Figures 21, 22, and 23 show the carbon intensity of electricity from coupled generation and batteries for, respectively, PV, wind, and fossil-based generators. These carbon intensities are estimated using the model from section 2.2. and the LCAs from sections 2.1 and 2.3. Figure 16 shows the linear correlation between coupled system carbon intensity and generator carbon intensity, and how storage technology affects that correlation.
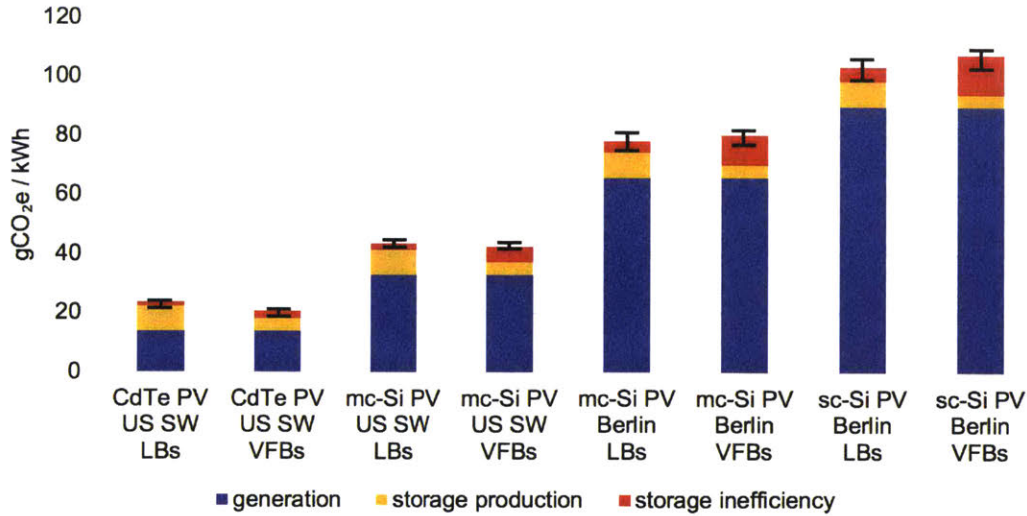
Figure 21. GHG emissions of power from different PV systems coupled with LBs or VFBs. PV systems differ by cell type and installation location. Other parameters match base case values in Figure 10. Bars indicate the difference between "best" and "worst" case scenarios for each storage technology. Best assumes the high values of efficiency and cycle life in Table 4, while worst assumes the low values. Fraction of generation sent to storage f is 50%, to correspond to the approximate upper bound of f needed to flatten intermittent generation across 24 hours, or conversely needed to convert constant fossil-based generation into peak supply.
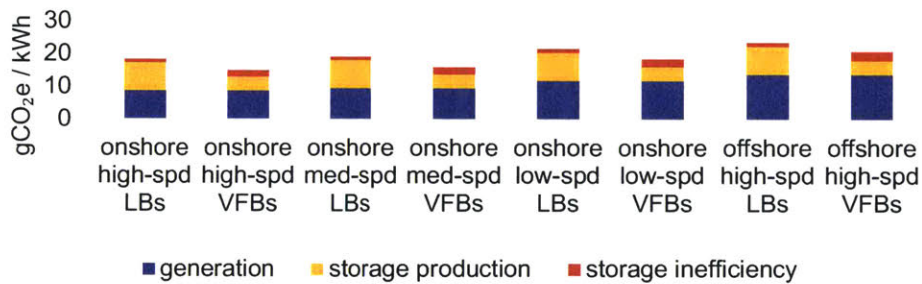

Figure 22. GHG emissions of power from different wind power systems coupled with LBs or VFBs. Wind systems differ by average local wind-speed and installation onshore or offshore. Other parameters match assumptions in Table 5. Bars indicate the difference between "best" and "worst" case scenarios for each storage technology. Best assumes the high values of efficiency and cycle life in Table 2, while worst assumes the low values. Fraction of generation sent to storage f is 50%, to correspond to the approximate upper bound of f needed to flatten intermittent generation across 24 hours, or conversely needed to convert constant fossil-based generation into peak supply.
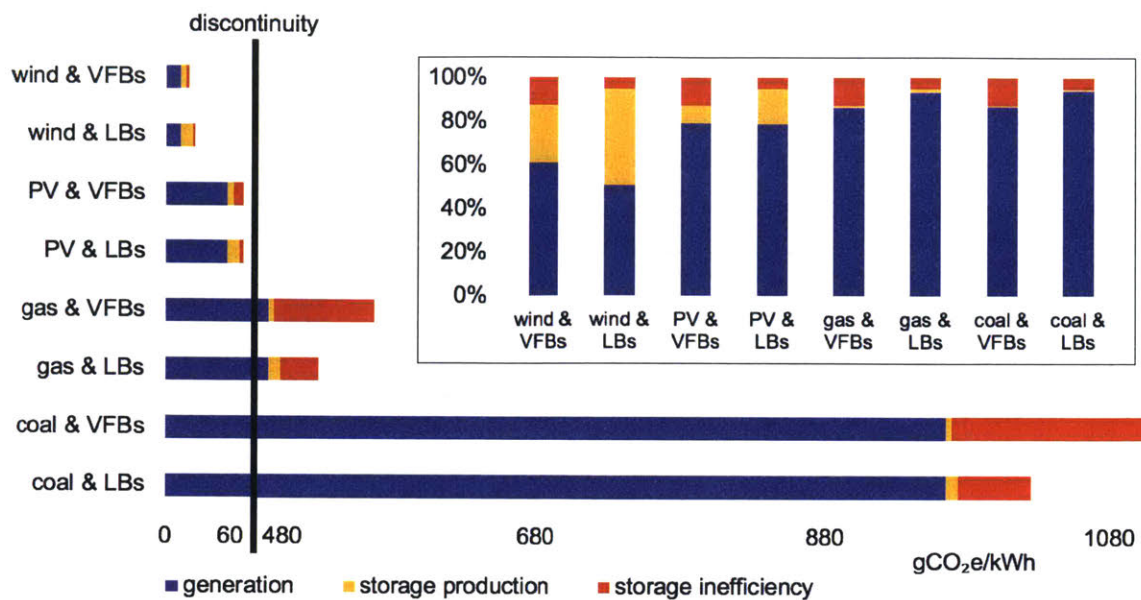
Figure 23. GHG emissions of power from different generators coupled with LBs and VFBs. PV cases assume installation in Sydney, Australia, and mc-Si cell type. Other PV parameters match base case values in Figure 8. Wind cases assume onshore installation in a medium wind-speed (~8 m/s) area. Other parameters match values in Table 4. Gas and coal cases assume typical CCNG and SCPC emissions values of 488 and 965 g_C/kWh, respectively [19]. Fraction of generation sent to storage f is 50%, to correspond to the approximate upper bound of f needed to flatten intermittent generation across 24 hours, or conversely needed to convert constant fossil-based generation into peak supply.
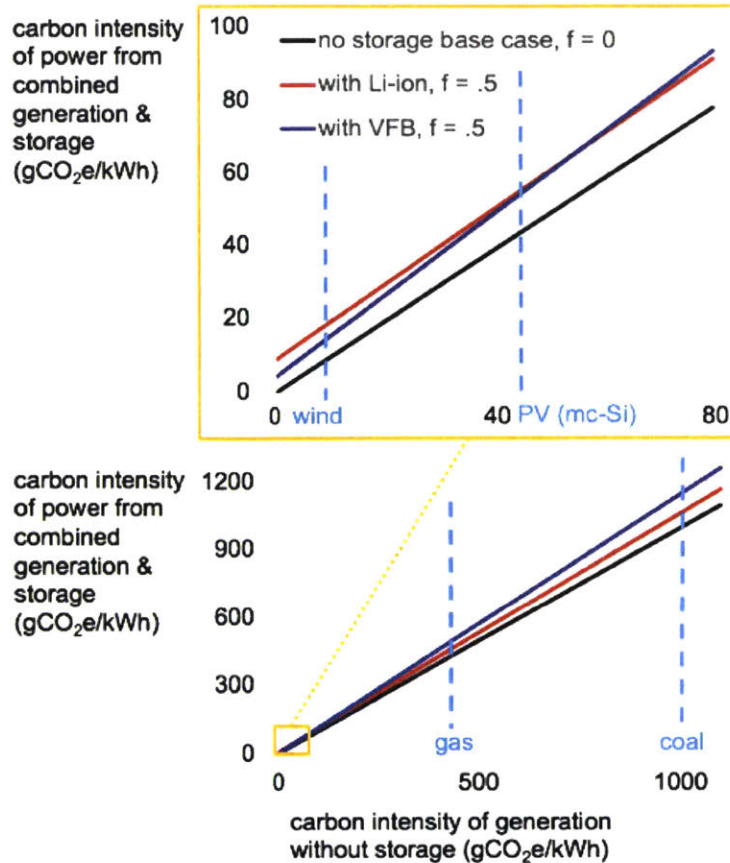
Figure 24. Carbon intensity of coupled generation and storage vs. carbon intensity of generation without storage. The wind, PV, gas, and coal numbers shown are respresentative of, respectively, onshore wind power in high wind-speed areas, mc-Si PV in Australia, combined cycle natural gas power, and super-critical pulverized coal. Equations (21) and (22) in section 3.2.2 describe the y-intersections and slopes of these carbon intensity lines.

3.2.2. Coupled generation and storage: discussion

The most important result is that, across all scenarios displayed, renewable electricity has much lower GHG emissions than fossil electricity. Figures 13-16 show this to hold true independent of: whether the renewable generator is PV or wind; whether the PV type is CdTe or crystalline silicon; whether the renewable generator is paired with no storage, LB storage, or VFB storage; and whether the renewable generator is located in northern Europe or the southern US. As seen in Figure 21, the most carbon-intensive mainstream PV power (sc-Si PV produced in China, installed in Berlin, and coupled with sufficient LBs to store 50% of it's generation) still emits only ~25% of the GHGs emitted by the least carbon intensive

mainstream fossil power (CCNG with no storage). Therefore, to understand the GHG emissions impacts of renewables, future work should not focus on more accurately accounting for GHGs from production of battery control systems or other system components. Whether wind power coupled with LBs emits 20 or 21 or even 40g$_C$/kWh, it is still an order of magnitude less carbon intensive than fossil generation without carbon capture. Instead, future work on renewables' emissions impacts should focus on consequential LCA, including questions of which generation types are most likely to be displaced by renewables deployment, dependent on location and economics, among other factors.

The percentage impact panel in Figure 23 illustrates another result: the storage parameter that controls emissions impact depends upon the generator to which the storage is coupled. Given low-emission generation, such as wind or CdTe PV, the storage feature that dominates emissions impact is storage production emissions (see orange sections in the left two bars of Figure 21). Given high-emission generation, such as gas or coal, the storage feature that dominates emissions impact is storage efficiency (see red sections in bottom four bars of Figure 23). One implication is that, if storage is being added to microgrids or regional grids with low-emission generation (I$_{avg}$ < 50 g$_C$/kWh), GHG emissions can be minimized by deploying storage products with the lowest production emissions. Conversely, if storage is being added to regions with high-emission generation (I$_{avg}$ > 200 g$_C$/kWh), GHG emissions can be minimized by deploying storage products with the highest efficiency.

Figure 24 illustrates the linear relationship between coupled system carbon intensity and generator carbon intensity. The parameters of the storage technology influence both the y-axis intersection and the slope of the line, according to the model equations in section 2.2.1:

$$y - axis\ intersection = \eta(e_s/E_{sT})/(DC) \ / \ (1/f - 1 + \eta) \tag{21}$$

$$slope = [1 - f(1 - \eta)] \tag{22}$$

These values are not particular to GHGs. Analogous qualitative behavior will thus hold for emissions of other pollutants, as well as "emissions" of dollars (costs/kWh). That is, emission and cost intensities of coupled systems, as a function of generator intensity, will have different slopes dependent on storage

technology. Choosing a specific storage technology for a coupled system can minimize emission (or cost) intensity for one generator type, but not for another.

4. Conclusion

This thesis first quantifies the impacts of previously explored variables on the carbon intensity of PV power, including irradiance, rated module efficiency, lifetime, and degradation. We then find that, compared to the impacts of these variables, (1) emissions impacts from temperature effects are significant in warm regions (order 10% increase), (2) emissions differences between Chinese and European PV manufacturing are significant (~25% difference), (3) emissions impacts from adding solar tracking are significant in some places (up to ±12% change) and negligible in others (±1%), and (4) impacts from inverter overloading are small (less than 2 g_C/kWh decrease). The analysis of overloading, tracking, and temperature effects demonstrates the benefit to PV life cycle assessment of incorporating more detailed models of PV performance. Potential improvements in our PV LCA model include incorporation of end-of-life emissions, future foreground LCIs, other PV technologies (e.g., bifacial modules), and transmission from generation-site to end-use site.

Relative to stationary mounting, solar tracking is found to decrease the GHG emissions of power from multi-crystalline silicon PV in most regions analyzed (by 0 to ~12%, or 0 to ~4 g_C/kWh), and to increase the emissions of power from cadmium telluride PV in most regions analyzed (by 0 to ~12%, or 0 to ~4 g_C/kWh). For any PV cell type, if the ratio of module production emissions to tracker production emissions increases in future, independent of absolute emission values, tracking will more commonly decrease PV carbon intensity. Conversely, if the ratio of module production emissions to tracker production emissions decreases, tracking will more commonly increase PV carbon intensity.

This thesis also presents a simple model for estimating emissions from integrated power generation and energy storage. The model applies to emissions of all pollutants, not only GHGs, and to all storage tech-nologies, including pumped hydroelectric and electrochemical storage. As a case study, the model is used to estimate the carbon intensity of electricity from systems that couple photovoltaic and wind gener-

ation with lithium-ion batteries (LBs) and vanadium redox flow batteries (VFBs). The case study of renewables and battery storage indicates that, even when coupled with large amounts of LBs or VFBs, PV and wind power remain much less carbon intensive than fossil-based generation. The most carbon intensive renewable power analyzed (sc-Si PV produced in China, installed at latitude corresponding to Berlin, and coupled with sufficient VFBs to store 50% of generation and thus provide flat baseload power supply to grid on most days) still emits only ~25% of the GHGs of the least carbon intensive mainstream fossil power (combined cycle natural gas turbine with no storage).

Lastly, we find that the pathway to minimize GHG emissions of power from a coupled system depends upon the generator: given low-emission generation (<50 g_C/kWh), the minimizing pathway is the storage technology with lowest production emissions (VFBs over LBs for our case study); given high-emission generation (>200 g_C/kWh), the minimizing pathway is the storage technology with highest round-trip efficiency (LBs over VFBs). The latter case applies to a majority of the world's power generation today.

Possible directions for future work that builds on this thesis include:

1) Applying the models developed, including the models of storage and tracking impact on emissions, to other pollutants, not only greenhouse gases.

2) Applying the coupled storage and generation model, in particular Eq. (9) and Table 3, to other non-battery technologies, including pumped hydroelectric storage.

3) Incorporating the "microscopic" renewable LCAs developed here into "macroscopic" emission assessments of electricity generation across whole regions and countries. Dr. Emre Gençer and others are conducting related work.

4) Researching why Chinese mc-Si PV manufacturing is more energy-intensive than European mc-Si PV manufacturing.

5) Re-evaluating PV degradation assumptions and their impacts on PV carbon intensity and environmental impacts. The All India PV Surveys in 2014 and 2016 [34] found that approximately half of ~800 modules surveyed at 25+ sites across the country had degradation rates over 2%/yr. This is

much higher than the 0.7%/yr value assumed in most PV LCAs and recommended by the IEA PV LCA guidelines. Dr. Sarah Kurtz and other NREL degradation experts have pointed to the All India Survey as the most comprehensive recent data on PV degradation. If silicon PV is really degrading at these higher rates, this could significantly increase the carbon intensity and other environmental impacts of PV power, as can be seen in Figure 11. We are currently corresponding with the survey authors to assess how representative the modules surveyed are of world-wide suppliers, e.g., how many come from Tier-1 manufacturers.

References
[1]   IEA. Energy, Climate Change & Environment. Paris, France: 2016.
[2]   The Energy Initiative MIT. The Future of Solar Energy: An interdiscipinary MIT study. Mit 2015:3–6. doi:10.1002/yd.20002.
[3]   GlobalData. Solar PV generation statistics, wind generation statistics, n.d.
[4]   ExxonMobil. 2017 Outlook for Energy: A View to 2040. 2017.
[5]   BNEF. Bloomberg New Energy Finance Report 2017. 2017.
[6]   Energy FI for S. Photovoltaics Report. 2017.
[7]   WindEurope. The European offshore wind industry - Key trends and statistics 2017. 2018.
[8]   EIA. Form EIA-860 : Annual Electric Generator Report 2016.
[9]   Leccisi E, Raugei M, Fthenakis V. The energy and environmental performance of ground-mounted photovoltaic systems - A timely update. Energies 2016;9. doi:10.3390/en9080622.
[10]   Garrett P, Rønde K. Life Cycle Assessment of Electricity Production from an onshore V90-3 . 0MW Wind Plant September 2012 Authors : Peter Garrett & Klaus Rønde Vestas Wind Systems A / S. Vestas Wind Syst A/S Vestas 2012:1–106.
[11]   Garrett P, Rønde K, Finkbeiner M. Life Cycle Assessment of Electricity Production from an onshore V110-2 . 0MW Wind Plant. Vestas Wind Syst A/S Vestas 2012:1–106.
[12]   Garrett P, Klaus R. Life Cycle Assessment of Electricity Production from a V100-1 . 8MW Gridstreamer Wind Plant 2011:105.
[13]   Razdan AP, Garrett P, Razdan AP, Garrett P. Life Cycle Assessment of Electricity Production from an onshore V100-2 . 0 MW Wind Plant 2015.
[14]   Siemens. Onshore wind power plant employing SWT-2.3-108. A Clean Energy Solut - from

Cradle to Grave 2014:16.

[15] Siemens. Onshore wind power plant employing SWT-3.2-113. A Clean Energy Solut - from Cradle to Grave 2014:16.

[16] Siemens. Offshore wind power plant employing SWT-4.0-130. A Clean Energy Solut - from Cradle to Grave 2014:16.

[17] Siemens. Offshore wind power plant employing SWT-7.0-154. A Clean Energy Solut - from Cradle to Grave 2014:16.

[18] Weinzettel J, Reenaas M, Solli C, Hertwich EG. Life cycle assessment of a floating offshore wind turbine. Renew Energy 2009;34:742–7. doi:10.1016/j.renene.2008.04.004.

[19] Skone TJ (National ETL. Power Generation Technology Comparison from a Life Cycle Perspective. Pittsburgh, PA: 2013.

[20] Finkbeiner M, Inaba A, Tan R, Christiansen K, Klüppel H-J. The New International Standards for Life Cycle Assessment: ISO 14040 and ISO 14044. Int J Life Cycle Assess 2006;11:80–5. doi:10.1065/lca2006.02.002.

[21] Peng J, Lu L, Yang H. Review on life cycle assessment of energy payback and greenhouse gas emission of solar photovoltaic systems. Renew Sustain Energy Rev 2013;19:255–74. doi:10.1016/j.rser.2012.11.035.

[22] Hsu DD, O'Donoughue P, Fthenakis V, Heath GA, Kim HC, Sawyer P, et al. Life Cycle Greenhouse Gas Emissions of Crystalline Silicon Photovoltaic Electricity Generation: Systematic Review and Harmonization. J Ind Ecol 2012;16. doi:10.1111/j.1530-9290.2011.00439.x.

[23] Frischknecht R, Heath G, Raugei M, Sinha P, de Wild-Scholten M, Fthenakis V, et al. Methodology Guidelines on Life Cycle Assessment of Photovoltaic Electricity, 3rd ed. IEA PVPS Task 12 Int Energy Agency Photovolt Power Syst Progr 2016.

[24] Dobos AP. PVWatts Version 5 Manual (NREL/TP-6A20-62641). 2014.

[25] Bayod-Rújula ÁA, Lorente-Lafuente AM, Cirez-Oto F. Environmental assessment of grid connected photovoltaic plants with 2-axis tracking versus fixed modules systems. Energy 2011;36:3148–58. doi:10.1016/j.energy.2011.03.004.

[26] Desideri U, Zepparelli F, Morettini V, Garroni E. Comparative analysis of concentrating solar power and photovoltaic technologies: Technical and environmental evaluations. Appl Energy 2013;102:765–84. doi:10.1016/j.apenergy.2012.08.033.

[27] Beylot A, Payet JÔ, Puech C, Adra N, Jacquin P, Blanc I, et al. Environmental impacts of large-scale grid-connected ground-mounted PV installations. Renew Energy 2014;61:2–6. doi:10.1016/j.renene.2012.04.051.

[28] Bolinger M, Seel J, LaCommare KH. Utility-Scale Solar 2016. 2017.

[29] Sinha P, Schneider M, Dailey S, Jepson C, De Wild-Scholten M. Eco-efficiency of CdTe photovoltaics with tracking systems. 39th IEEE Photovolt. Spec. Conf., Tampa, FL, US: 2013.

[30] Perpiñan O, Lorenzo E, Castro MA, Eyras R. Energy payback time of grid connected PV systems: Comparison between tracking and fixed systems. Prog Photovoltaics Res Appl 2009;17:137–47. doi:10.1002/pip.871.

[31] Nian V. Impacts of changing design considerations on the life cycle carbon emissions of solar photovoltaic systems. Appl Energy 2016;183:1471–87. doi:10.1016/j.apenergy.2016.08.176.

[32] Laboratories SN. PV Performance modeling collaborative (PVPMC) website n.d. https://pvpmc.sandia.gov (accessed December 1, 2017).

[33] Jordan DC, Kurtz SR, VanSant K, Newmiller J. Compendium of photovoltaic degradation rates. Prog Photovoltaics Res Appl 2016;24:978–89. doi:10.1002/pip.2744.

[34] Chattopadhyay S, Dubey R, Kuthanazhi V, Zachariah S, Bhaduri S, Mahapatra C, et al. All-India Survey of Photovoltaic Module Reliability: 2016. Mumbai, India: 2017.

[35] Sivaram V, Kann S. Solar power needs a more ambitious cost target. Nat Energy 2016. doi:10.1038/nenergy.2016.36.

[36] Zhuk A, Zeigarnik Y, Buzoverov E, Sheindlin A. Managing peak loads in energy grids: Comparative economic analysis. Energy Policy 2016. doi:10.1016/j.enpol.2015.10.006.

[37]   Krieger EM, Casey JA, Shonkoff SBC. A framework for siting and dispatch of emerging energy resources to realize environmental and health benefits: Case study on peaker power plant displacement. Energy Policy 2016. doi:10.1016/j.enpol.2016.05.049.

[38]   Denholm P, Hand M. Grid flexibility and storage required to achieve very high penetration of variable renewable electricity. Energy Policy 2011. doi:10.1016/j.enpol.2011.01.019.

[39]   Simon B, Finn-Foley D, Gupta D. GTM Research/ESA U.S. Energy Storage Monitor. 2018.

[40]   Yang G. Move over, lithium ion: Vanadium flow batteries finally become competitive for grid-scale energy storage. IEEE Spectr 2017.

[41]   Spanos C, Turney DE, Fthenakis V. Life-cycle analysis of flow-assisted nickel zinc-, manganese dioxide-, and valve-regulated lead-acid batteries designed for demand-charge reduction. Renew Sustain Energy Rev 2015. doi:10.1016/j.rser.2014.10.072.

[42]   Rydh CJ, Sandén BA. Energy analysis of batteries in photovoltaic systems. Part I: Performance and energy requirements. Energy Convers Manag 2005. doi:10.1016/j.enconman.2004.10.003.

[43]   Denholm P, Kulcinski GL. Life cycle energy requirements and greenhouse gas emissions from large scale energy storage systems. Energy Convers Manag 2004. doi:10.1016/j.enconman.2003.10.014.

[44]   Mitavachan H, Derendorf K, Vogt T. Comparative life cycle assessment of battery storage systems for stationary applications. Environ Sci Technol 2015. doi:10.1021/es504572q.

[45]   Miller I, Gençer E, Vogelbaum HS, Brown PR, Torkamani S, O'Su. Parametric modeling of life cycle greenhouse gas emissions from photovol-taic power. [Under Rev 2018.

[46]   ISO 14040. The International Standards Organisation. Environmental management — Life cycle assessment — Principles and framework. ISO 14040 2006;2006:1–28. doi:10.1136/bmj.332.7550.1107.

[47]   Steubing B, Wernet G, Reinhard J, Bauer C, Moreno-Ruiz E. The ecoinvent database version 3 (part II): analyzing LCA results and comparison to version 2. Int J Life Cycle Assess 2016. doi:10.1007/s11367-016-1109-6.

[48]   Jungbluth N, Stucki M, Flury K, Frischknecht R, Büsser S. Life Cycle Inventories of Photovoltaics. Ulster, CH: 2012.

[49]   Frischknecht R, Itten R, Sinha P, de Wild-Scholten M, Zhang J, Fthenakis V. Life cycle inventories and life cycle assessment of photovoltaic systems; Report IEA-PVPS T12-04:2015. Paris, France: 2015.

[50]   Jean J, Brown PR, Jaffe RL, Buonassisi T, Bulović V. Pathways for solar photovoltaics. Energy Environ Sci 2015;8:1200–19. doi:10.1039/c4ee04073b.

[51]   Pachauri RK, Allen MR, Barros VR, Broome J, Cramer W, Christ R, et al. Climate Change 2014: Synthesis Report. Contribution of Working Groups I, II and III to the Fifth Assessment Report of the Intergovernmental Panel on Climate Change. 2014. doi:10.1017/CBO9781107415324.

[52]   Wild-scholten MJM De. Life Cycle Assessment of PV Status 2011, Part 1 Data Collection. Groet, Netherlands: n.d.

[53]   IEA IEA. CO2 Emissions from Fuel Combustion 2017 - Highlights. Int Energy Agency 2017. doi:10.1787/co2_fuel-2017-en.

[54]   Gilman P, Dobos A, DiOrio N, Freeman J, Janzou S, Ryberg D. SAM Photovoltaic Model Technical Reference Update. 2018.

[55]   Cui Y, Du C, Yin G, Gao Y, Zhang L, Guan T, et al. Multi-stress factor model for cycle lifetime prediction of lithium ion batteries with shallow-depth discharge. J Power Sources 2015. doi:10.1016/j.jpowsour.2015.01.003.

[56]   Alsaidan I, Khodaei A, Gao W. A Comprehensive Battery Energy Storage Optimal Sizing Model for Microgrid Applications. IEEE Trans Power Syst 2018. doi:10.1109/TPWRS.2017.2769639.

[57]   Eaton CT. AC vs. DC coupling in utility-scale solar plus storage projects 2016.

[58]   Garrett P, Ronde K. Life Cycle Assessment of Electricity Production from an onshore V90-2.6 MW Wind Plant 2013:107.

[59]   Razdan AP, Garrett P, Razdan AP, Garrett P, Razdan AP, Garrett P. December 2015 Life Cycle

Assessment of Electricity Production from an onshore V110-2 . 0 MW Wind Plant December 2015 Authors : Priyanka Razdan , Peter Garrett Vestas Wind Systems A / S Vestas Wind Systems A / S 2015.

[60]   GWEC. Global Wind Statistics 2016. 2017. doi:10.2.2017.

[61]   Siemens. Offshore wind power plant employing SWT-6.0-154. A Clean Energy Solut - from Cradle to Grave 2014:16.

[62]   Laboratory UNRE. System Advisor Model website n.d. https://sam.nrel.gov/weather (accessed March 1, 2018).

[63]   Solar J. Download center poly-module datasheets n.d. https://www.jinkosolar.com/down-load 356.html (accessed February 1, 2018).

[64]   Trina Solar. Products & solutions downloads: multicrystalline datasheets n.d. http://trinasolar.com (accessed February 1, 2018).

[65]   JA Solar. PV module> Main Module > multicrystalline download n.d. http://www.jasolar.com/Standard/113-JAM6%2528K%2529-60%252F4BB#level-1 (accessed February 1, 2018).

[66]   Sea-Distances. Port distances calculator n.d. https://sea-distances.org (accessed December 1, 2017).

[67]   Gagnon P, Margolis R, Melius J, Phillips C, Elmore R. Rooftop solar photovolatic technical potential in the united states: A detailed assessment. Nrel 2016:82. doi:https://www.nrel.gov/docs/fy16osti/65298.pdf.

Appendix A - PVWatts PV performance model

This section provides an outline of PVWatts' performance model. Some of the equations below appear in the PVWatts technical manual [1], but many do not and are only referenced or implied. Given that a central contribution of this thesis is incorporating modern PV performance modeling into PV LCA, it is important to clearly define the performance model used.

In PVWatts, the instantaneous AC power output of a PV system is given by:

$$P_{AC} = A \times I \times \eta \times \eta_{inv} \times \prod_i (1 - f_{loss,i}) \tag{A.1}$$

where I is irradiance transmitted across the PV modules' glass surface (kW/m^2), η is module operating efficiency, η_{inv} is inverter efficiency, and $f_{loss,i}$ are fractions of DC power lost to certain system features. Irradiance, module efficiency, and inverter efficiency are expanded in Tables A.1, A.2, and A.3. System features that do not affect these three terms and are assumed by PVWatts to cause constant DC power losses are represented by the $f_{loss,i}$. These include electrical resistance (assumed 2.5% loss), manufacturing and installation imperfections (2%), rating inaccuracy (1%, adjusted by SoLCAT to 0% for CdTe), and availability (3%). More detail on PV performance modeling can be found in PVWatts' technical documentation [1], the website for Sandia National Laboratories' PV Performance Modeling Collaborative [2], and the references in Tables A.1-A.3.

Table A.1

Expansion of efficiency term in PVWatts performance model (equation (A.1))
(Location-dependent weather data in red.)

Term	Description	Expansion
η	Module operating efficiency, fraction of transmitted irradiance converted to DC power in module	$\eta = \eta_{STC} \times (1 + \gamma \times (T_{cell} - 25ºC)) \times (1 - f_{LID})$
γ	Thermal coefficient, change in operating efficiency per unit change in cell temperature, reversible.	$\gamma = -0.47\,\%/ºC$ for silicon PV $\gamma = -0.20\,\%/ºC$ for CdTe PV PVWatts assumed values, based on statistical analysis of >11000 modules. See p4 & p9 of [1]
f_{LID}	Fraction of efficiency lost to light-induced degradation (LID) when modules are first exposed to extended sunlight.	$f_{LID} = 0.015\ (1.5\%)$ PVWatts silicon-based assumed value. SoLCAT adjusts LID to 0% for CdTe
T_{cell}	Cell temperature	$T_{cell} = T_{cell,0}\, e^L + \dfrac{\left[\alpha \Delta I + (1 - e^L)\left(\alpha\left(I_0 + \frac{\Delta I}{L}\right) + \Sigma_i h_i T_i\right)\right]}{\Sigma_i h_i}$ where $T_{cell,0}$ is cell temp. at prior time step; α is module absorptivity; I_0 is irradiance at prior time step; T_i are ambient temp., sky temp., and ground or roof temp.; h_i are convective coefficient to air, radiative coefficient to sky, and radiative coefficient to ground or roof; and L is ratio of convection to capacitance $(\Delta t\, \Sigma_i h_i / (\rho_A c_p))$;. Each parameter can be further expanded, such that T_{cell} = function (prior cell temp., ambient temp., irradiance (prior & current), wind speed, and mounting type) For elaboration see [3] starting on p4.

Table A.2
Expansion of irradiance term in PVWatts performance model (equation (A.1)).
(Location-dependent weather data in red.)

Term	Description	Expansion
I	Irradiance crossing PV module surface	$I = I_{POA} \times (1 - f_{sh,pvw}) \times (1 - f_{soil}) \times (1 - f_{reflect})$
$f_{sh,pvw}$ f_{soil}	Fractions of irradiance blocked by shading and soiling, respectively	$f_{sh,pvw} = .03$ (3%) , PVWatts assumed value° $f_{soil} = .02$ (2%), PVWatts assumed value
$f_{reflect}$	Fraction of irradiance reflected off module surface	$f_{reflect}$= function (angle between incident irradiance and module surface, material properties including glass thickness and index of refraction) See "Physical IAM Model" section of [2] for function form.
I_{POA}	Irradiance incident on module surface with no shading, soiling, or reflection	$I_{POA} = I_{direct} + I_{diff.sky} + I_{diff.gr}$
I_{direct}	Component of sun beam irradiance normal to module surface	$I_{direct} = I_{DNI} \times cos(\theta_{AOI})$
I_{DNI}	Direct normal irradiance, also called sun beam irradiance	Provided by hourly weather data
θ_{AOI}	Angle of incidence, the angle between sun beam and normal of module surface	θ_{AOI} = function (day of year, time of day, latitude, longitude, altitude, module tilt (θ_{tilt}), module azimuth). For 1-axis tracking, θ_{tilt} = function (day of year, time of day, latitude, longitude) and rotates between -45° and +45° according to [4]. See "AOI" section of [2] for function forms.
$I_{diff,sky}$	Diffuse irradiance from sky incident on module plane	$I_{diff,sky} = I_{DHI} \times [(1 + cos(\theta_{tilt}))/2 \times a + b + c]$ See "Perez Sky Diffuse" section of [2] for a b & c .
I_{DHI}	Diffuse irradiance incident on horizontal plane	Provided by hourly weather data
$I_{diff.gr}$	Irradiance incident on module plane that is reflected off ground	$I_{diff.gr} = I_{GHI} \times albedo \times (1 - cos(\theta_{tilt}))/2$
I_{GHI}	Global horizontal irradiance	$I_{GHI} = I_{DHI} + I_{DNI} \times cos(\theta_{sun})$
albedo	Fraction of irradiance reflected off ground	Provided by hourly weather data, or set to 0.2 by PVWatts if data unavailable

---

[7] For fixed-tilt systems, PVWatts does not model self-shading by modules or utilize the ground coverage ratio (GCR) input. For systems with 1-axis tracking, PVWatts does model self-shading using the GCR input. Our model and SoLCAT do not use this feature. We first set the PVWatts input GCR to 0.001, corresponding to negligible self-shading, and then use empirically based derates to account for self-shading and other shading losses. As indicated in the main body, 2.5% for utility-scale PV and 7% for rooftop PV are typical shading losses, based on the online PVWatts manual [1] and an NREL report on PV and shading [5].

Table A.3
Expansion of inverter efficiency term in PVWatts performance model (equation (A.1)).

Term	Description	Expansion
η_{inv}	Inverter efficiency, fraction of theoretical DC power entering inverter (given zero voltage adjustment by inverter) that is converted to AC power $\eta_{inv} = P_{AC,inv}/P_{DC,inv,0}$	If $P_{DC,inv,0} < c_{DC,inv}$, (regular efficiency "hockey" curve) $$\eta_{inv} = .9858 - .0162 \times \left(\frac{P_{DC,inv,0}}{c_{DC,inv}}\right) - .0059 \times \left(\frac{c_{DC,inv}}{P_{DC,inv,0}}\right)$$ If $P_{DC,inv,0} \geq c_{DC,inv}$ ("clipping") $\eta_{inv} = c_{AC,inv}/P_{DC,inv,0}$ thus $P_{AC,inv} = \eta_{inv}P_{DC,inv,0} = c_{AC,inv}$ This conditional models typical PV inverters that limit input DC power to their DC capacity by adjusting voltage.
$c_{DC,inv}$	Rated DC capacity of inverter	$c_{DC,inv} = c_{AC,inv}/\eta_{inv,reference}$ PVWatts assumes rated inverter efficiency $\eta_{inv,reference} = .96$
$P_{DC,inv,0}$	Theoretical DC power entering inverter, given zero voltage adjustment by inverter. If $P_{DC,inv,0} < c_{DC,inv}$ $P_{DC,inv} = P_{DC,inv,0}$ real = theoretical If $P_{DC,inv,0} \geq c_{DC,inv}$ ("clipping") $P_{DC,inv} = c_{DC,inv}$ real = capacity	$$P_{DC,inv,0} = P_{DC,panel} \times \prod_i (1 - f_{loss,i})$$ $$= A \times I \times \eta \times \prod_i (1 - f_{loss,i})$$

Equation (A.1) and its component equations in Tables A.1-A.3 give instantaneous power (P_{AC}). The location input to SoLCAT determines the weather data used by PVWatts to calculate power at each time-step: direct normal irradiance, diffuse horizontal irradiance, ambient temperature, wind speed, and, if available, albedo. The weather data contains 8760 1-hour time steps, with different months' data selected from different years to compose a "typical" year of hourly data. PVWatts calculation of time-averaged AC power ($\overline{P_{AC}}$) thus entails 8760 calculations of instantaneous power. In addition to [1], detail on weather data can be found in [6] and [7]. Dividing time-averaged AC power by rated DC module capacity gives year-1 DC capacity factor:

$$CF_{pvw} = \overline{P_{AC}}/c_{DC} \tag{A.2}$$

Appendix References

[1] Dobos AP. PVWatts Version 5 Manual (NREL/TP-6A20-62641). 2014.

[2] Sandia National Laboratories. PV Performance modeling collaborative (PVPMC) website, https://pvpmc.sandia.gov; 2017 [accessed 1 December 2017]

[3] Fuentes, MK. (1987). A Simplified Thermal Model for Flat-Plate Photovoltaic Arrays. SAND85-0330. Albuquerque, NM: Sandia National Laboratories. Accessed September 3, 2013: http://prod.sandia.gov/techlib/access-control.cgi/1985/850330.pdf.

[4] Marion, W.; Dobos, A. P. (2013). Rotation Angle for the Optimum Tracking of One-Axis Trackers. TP-6A20-58891. Golden, CO: National Renewable Energy Laboratory.

[5] Deline C, Meydbray J, Donovan M. Photovoltaic Shading Testbed for Module-level Power Electronics: 2014 update. NREL Tech Rep NREL/TP-5200-57991 2012:32. doi:NREL/TP-5200-54876.

[6] US National Renewable Energy Laboratory. System Advisor Model weather webpage, https://sam.nrel.gov/weather; 2018 [accessed 1 March 2018]

[7] Gilman P, Dobos A, DiOrio N, Freeman J, Janzou S, Ryberg D. SAM Photovoltaic Model Technical Reference Update. 2018.